

Review on process model, structure-property relationship of composites and future needs in fused filament fabrication

Journal of Reinforced Plastics and Composites
2020, Vol. 39(19–20) 758–789
© The Author(s) 2020
Article reuse guidelines:
sagepub.com/journals-permissions
DOI: 10.1177/0731684420929757
journals.sagepub.com/home/jrp


Easir Arafat Papon  and Anwarul Haque

Abstract

This paper presents the state-of-the-art of additive manufacturing of composites for processing functional, load-bearing components. A general overview of different additive manufacturing methods is provided, and specific attention is focused on fused filament fabrication-based composites processing. Different process modeling strategies are summarized, and key aspects of these models are discussed. Significant results such as thermal and fluid flow characteristics, effects of nozzle geometry on melt flow, fiber orientation, bead spreading, and solidification, the formation of residual stresses, and deformation behavior are discussed from computational modeling perspective. The scientific advancement, model limitations, and future modeling needs are prescribed reviewing the current works. A general overview of material development in nano-micro-macro-scale reinforcement is also presented. Different length-scales of reinforcement has its own challenges and promises. The continuous fiber reinforcement has a great potential for being the next-generation composites manufacturing technology. However, the challenges in reducing the void content, better bonding between the fiber–matrix, and layer-layer adhesion, and process uncertainty are some of the key areas yet to advance. Based on the current limitations on computational modeling, materials development, and process modeling studies, future research needs and recommendations are provided.

Keywords

Additive manufacturing, fused filament fabrication, computational modeling, mechanical properties, fiber reinforced polymer composites

Introduction

Additive manufacturing (AM) of polymers and composites is a rapidly growing area in processing prototype parts, complex geometries, smart materials, and functionally graded components in recent years. It is a layer by layer integration of functional materials from a three dimensional (3D), computer-aided design model offering reduced material waste and little to no post-processing steps. Such advantage makes AM a unique substitution to the traditional subtractive manufacturing processes like compression molding and injection molding. AM also brings out the possibility for multi-functional applications by entailing not only the seamless integration of dissimilar materials but also the embedding of functional components and nano to micro-scale reinforcements in a tailorable paradigm. Today, the technology has progressed a lot further

since the first patent of it by Hull.¹ Since then, different AM methods for different material types like powders, polymers, ceramics and metals have been developed and is under continuous improvement to bring out its potential in composites fabrication by different researchers around the world. Among the various available AM methods, Powder-liquid 3D printing technology (3DP) was first developed by the Massachusetts Institute of

Advanced Composite Materials Laboratory, Department of Aerospace Engineering and Mechanics, The University of Alabama, Tuscaloosa, USA

Corresponding author:

Easir Arafat Papon, Advanced Composite Materials Laboratory, Department of Aerospace Engineering and Mechanics, The University of Alabama, Tuscaloosa, AL 35487, USA.
Email: mpapon@ua.edu

Technology (MIT) researchers.² Followed by MIT, laminated object manufacturing (LOM)³ with plastic laminate, stereolithography apparatus (SLA) using photopolymer liquid binder, selective laser sintering (SLS)⁴ with plastic powders and material extrusion⁵ using plastic filaments were developed subsequently.

In the 3DP process, the material is provided in the powder form and then selectively joined layer by layer using a liquid binder. The process has its own advantage of making the parts with a high-quality surface finish. However, slow printing, higher porosity, and inferior bonding quality are few of the drawbacks of the 3DP process. The LOM is based on the layer by layer cutting, and lamination of sheets of polymers, prepreg composites, ceramics, and metal filled tapes and these are thermally bonded together for the construction of the complete part. Although high-strength parts can be manufactured in LOM with preferred laminate orientation, the process entails lots of material wastage and also not very suitable for making complex shapes. The SLA uses thermoset-polymer resins with photoactive monomers in it and cured by UV-activation or focused electron beam. The polymerization, resin curing, and solidification take place almost instantly through the UV-heating to give the preferred shape in a layer by layer fashion. This method has immense potential in processing complex structural-nanocomposites.⁶ However, the challenges lie on material availability, tailoring the viscoelastic property of the materials, reinforcement-matrix bonding, and void contents. On the other hand, SLS utilizes almost a similar technique like 3DP with the only exception that the 3DP uses liquid binder for bonding the powder particles, whereas SLS uses controlled laser beam to sinter and bind the powders. The quality of the parts largely depends on the particle size and laser-scanning process parameters. Similar to SLA, the SLS also has great potential for nanocomposites,⁷ apart from the issues like the limited material availability, poor reinforcement-matrix bonding, a higher amount of void contents, the orientation of reinforcement, and poor surface finish. Finally, the fused filament fabrication (FFF), also known under the trademark term fused deposition modeling (FDMTM) is one of the most popular extrusion-based AM process⁸ having a great potential for both nanoscale, discontinuous, and continuous fiber reinforced polymer (CFRP) composites, in a wide variety of applications, ranging from small scale prototyping to large-scale industrial products.⁹ The FFF extrusion-head can deposit a semi-molten material according to a computerized and pre-defined pattern on a two-dimensional plane (x-y plane). The as-built two-dimensional patterns are then stacked layer-by-layer along the build direction (z-axis) to give a complete 3D shape.¹⁰

The above mentioned 3D printing methods are researched to understand the feasibility and benefits in terms of processing fiber-reinforced composites. Short and discontinuous fiber reinforced composites (FRC) are used in all the available methods including LOM, SLA, SLS, FFF, etc. In SLA, E-glass, carbon fiber, and para aramid fiber were used with photocurable resins where E-glass was found to increase both the tensile strength and stiffness in comparison to the neat resin.¹¹ SLS is one of the more mature technologies that has been studied for short and nanoparticle reinforced composites. The addition of carbon nanofiber (CNF) into polyimide-12 (PA-12),¹² short carbon fibers (SCF) into PA-12,¹³ graphene, and CF into polyether ether ketone (PEEK)^{14,15} were found to increase the tensile strength and modulus of the composites. LOM is used to successively cut prepreg composite sheets and then the sheets are bonded under a consolidation roller system. The technology has been used for both short and continuous fiber reinforcement. A very high tensile and flexural strength are achieved in this process for CFRP composites.¹⁶ FFF has been most widely used so far for nano-micro-macro particle reinforced and continuous fiber reinforced thermoplastic composites, which is the focus of this review. This technology has been used for both commercial establishments and in the research community due to its process simplicity and flexibility in materials development. Apart from the enormous potential in processing high-strength and high-stiffness composite parts rapidly with the added advantage of very high fiber alignment, FFF also has its intrinsic drawbacks like all other AM processes. The poor bonding, dimensional inaccuracy, anisotropy, and higher void contents are the critical challenges in FFF-based composites.

It is well established from the above discussion that the fundamental challenges in AM are more or less similar to all the available methods. A proper physical understanding of each of the process parameter is needed to address the challenges and relevant defense mechanism needs to be developed through coupled numerical-experimental modeling techniques. Apart from conducting the experiments, different software companies like Ansys[®],¹⁷ Digimat[®],¹⁸ and Dassault Systems[®],¹⁹ are updating their software packages for simulating complex thermodynamic processes in AM.

To date, the FFF system has been developed more promisingly than the other polymer-AM processes in terms of processing large scale, load-bearing composite parts. Oak Ridge National Laboratory in collaboration with Cincinnati Incorporated[®] has been the leader of large-scale ($6 \times 3 \times 1.8 \text{ m}^3$) 3D-printed composite manufacturing²⁰ called big area additive manufacturing (BAAM). BAAM setup is similar to FFF/FDMTM in principal, however, instead of melting a thin

filament, it operates a single-screw extruder to melt the pelletized feedstock similar to that used in injection molding. The composite additive manufacturing research instrument by Purdue University,²¹ large-scale additive manufacturing (LSAM) by Thermwood Incorporated²², and custom-made extrusion system by Baylor University in collaboration with Strangpresse LLC²³, are some of the efforts on expanding the capabilities for structural applications. Such technological advancements in manufacturing fields are very promising, however, the technology must provide end-user products with sufficient mechanical integrity and functional capabilities for sustainability. The weak interfacial bonding between the deposited layers, fiber–matrix interface, and anisotropy in material properties, process uncertainty, and higher amount of void contents in FFF are the critical issues that need to be addressed from physics perspective for the technology to be comparable with the tradition manufacturing processes. The distribution, size, and shape of the voids generated in FFF are random and highly depends on the processing parameters that result in a greater range of variabilities in the properties of the manufactured part. Due to various sources of uncertainties from the initial phase of filament extrusion to melting the filament, deposition of the molten layers, and solidification; it is highly unlikely to repeat the process with the higher build quality. Apart from that, the FFF process involves the layer-by-layer stacking sequences where the reinforcing agents can only be laid along the in-plane direction. Therefore, delamination is likely to occur in between the layers if the layer-wise bonding and fiber–matrix bonding are not perfect. Thus, the complexity increases for multi-phase materials, where the fiber–matrix bonding and void contents play major roles in the strength, toughness, and anisotropy. As of now, the trial-and-error approach is usually adopted to get a product with higher structural integrity and confidence. Different research initiatives like process optimization, numerical model development, multi-axis printing, surface functionalization, and bead to bead strengthening have been considered so far to address such issues. This is a major research area to address for the widespread application of FFF-AM based composites.

A good number of review articles are published in last few years discussing the available AM methods for processing composites,²⁴ advances in AM materials, methods and applications,^{25–28} effects of FFF process parameters on mechanical properties,²⁹ and optimization of process parameters for composites.³⁰ Very recently, an article is published³¹ with special attention on the physics of the FFF process and the mechanical properties of different composite systems. However, a complete and current state-of-the-art of numerical modeling strategies on FFF is missing in the literature.

This article presents a complete summary of the fluid flow and thermodynamics related studies at different stages of the FFF printing process, combining both single-phase polymer, and two-phase-discontinuous and continuous FRC. The physics of the process is discussed first, and then an overview of the numerical models are presented from the perspectives of melt flow, layer deposition, solidification, bonding, and its effects on the material anisotropies. Based on the modeling studies, a summary of the most recent two-phase material properties of nano-micro-macro scale reinforcement is discussed, and relevant process modeling studies are also reviewed. Finally, the article is concluded with an insight into the research gap, the future research direction of the FRC, and a few recommendations.

FFF-composite extrusion and associated physics

In FFF, the material is deposited along the x-y plane as continuous, single beads. The beads are of specific thickness and cross-sectional shapes, depending on the FFF process parameters and extruder-head geometric configurations. The as-printed beads adhere to the surrounding beads to accumulate a layer of beads depending on its solidification characteristics. Once a layer is printed, the z-height is changed, and the similar layering is continued for the layer by layer stacking sequences. This bead to bead adhesion approach (x-y, x-z, y-z bonding) has a significant impact on the dimensional accuracy and mechanical properties of the printed parts.

This section describes different steps, its related physics, and a detailed explanation of its effects on parts quality to understand the extrusion process, particularly for fiber-reinforced polymers. Figure 1 shows the complete picture of the FFF-extrusion and the effects of different geometric and process parameters on the effectiveness of the overall process.

Typically, an amorphous polymer or two-phase composite filament of a certain diameter is fed into the extrusion chamber through a motor-control mechanism. The mechanism pedals the initial solid-material feed rate and melt-extrusion rate. If the initial feed rate is not compatible to the physical behavior like melt temperature, heat capacity, and viscosity of the material and exceeds a certain critical limit, it can induce a compressive force on the filament and results in buckling prior entering the heating zone.³² The filament starts changing its phase to a glassy state as it enters into the heating zone, and transforms into a fully melted form prior to extrusion through the exit-nozzle. The metallic-heating chamber and nozzle

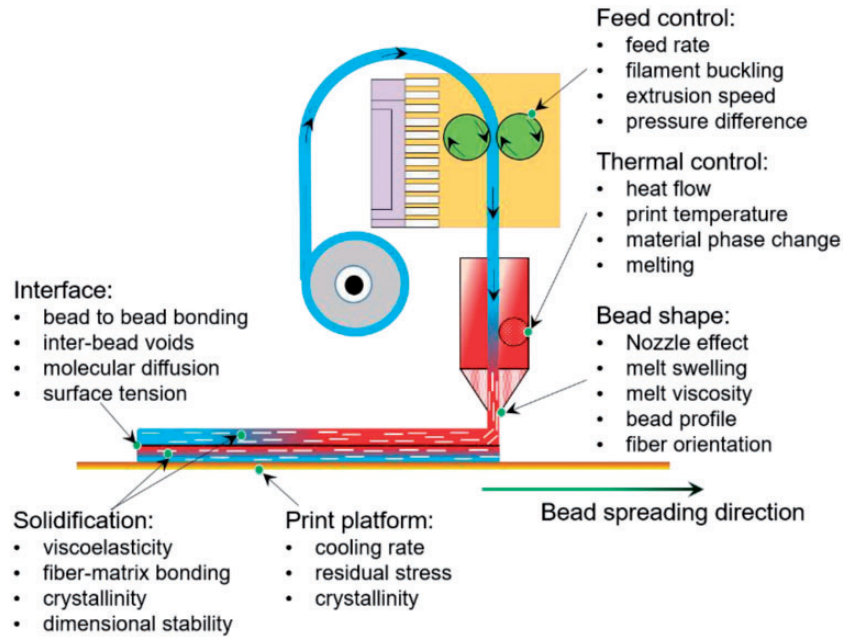


Figure 1. Schematic of the FFF process and associated process variables.

section usually has good thermal conductivity and ensures even temperature distribution inside the nozzle.³³ Thus, when the melt exits the nozzle, it reaches to the free environment with a uniform melt temperature and a parabolic flow field at the nozzle-outlet. At this stage, the effect of nozzle converging angle, exit-cross-sectional shape, and exit-velocity is very important to define the extruded-bead shape. This factor controls the melt swelling phenomenon³⁴ and changes the deposited bead shape on the print platform or previously deposited bead. If the filament is a fiber-reinforced composite, the orientation of fibers due to the shear alignment also takes place simultaneously at the nozzle-outlet and hence, controls the mechanical anisotropy of the printed beads. The reinforcing materials change the viscous response and bead-flow field^{34,35} and thus melt swelling and extruded-bead shape too. Therefore, the bead flow profile and fiber alignment are mutually inclusive and depend on each other.

The solidification phase starts as soon as the bead is in the open environment, on the print platform, or previously deposited bead. The temperature difference between the incoming bead, associated environment, and print platform governs the solidification process. The convective heat losses between the bead and print platform and radiative heat losses on external surfaces of the bead drive the solidification process. If the cooling rate exceeds a critical limit, the bead solidifies too quickly, resulting a low level of crystallinity and low molecular diffusion. In the case of a semi-crystalline material, such changes in crystallinity change the mechanical and thermal properties of the material.

However, when the cooling rate is extensively low, the transition from viscous fluid to a viscoelastic solid takes longer duration causing sagging of the material due to gravity effect and transforms to an undesirable bead shape.^{31,36} Thus, maintaining a favorable cooling rate is critical for the success of the FFF printing. As the bead solidifies, it also starts shrinking depending on its thermal expansion coefficient. While shrinking, residual stresses start to evolve that further promotes the shape deformation and dimensional inaccuracy.^{37,38}

In the case of a second bead that is to be deposited on to a previously deposited bead, the inter-bead bonding now comes into play. While the solidification and shape changes are already in place for the previously deposited one, the newly deposited bead demands a better contact surface with sufficient surface temperature for good inter-bead bonding and molecular inter-diffusion.³⁹ The longer exposure of the interface to a favorable temperature promotes good molecular coalescence, good inter-diffusion through the interface, and less inter-bead void spaces. Such bonding is governed by the surface tension of the material with a strong dependence on the cooling rate and viscosity. If the cooling rate is high enough, the molecular mobility of the adjacent beads are arrested, and poor inter-bead bonding is the result as an outcome. Again, if the cooling rate is too low, molecular interaction may be sufficient but at the cost of dimensional accuracy. Hence, a very precise thermal and fluid flow control is desired for a good FFF-printing. Also, the reinforcing materials highly affect the thermal and flow characteristics by adding extra complexity to the system.

All of these different sources collectively induce anisotropy both in the mechanical and thermal properties. The observed variation and anisotropy in properties will be discussed in Section “Future needs in FFF.” Hence, for the successful integration of the FFF process into industrial settings, understanding the complexities and modeling of this behavior accurately is very important.

Numerical modeling of FFF process

The computational domain of the FFF process can be classified into two stages. The thermal and fluid flow characteristics of the material inside the heating zone (liquefier) where the material is heated, melted, and flown through a confined liquefier, is the first stage. The flow characteristics also depend on the liquefier and nozzle heat capacities and thermal characteristics of the fluid material. In the second stage, the fluid comes out of the nozzle as a fully melted form, swells due to sudden pressure change, gets deposited on a platform, and starts solidifying due to the temperature difference. This stage is crucial as it defines the shape of the extruded bead, inter-bead bonding, residual stresses,³⁸ and shear-induced alignment^{40,41} of reinforcing materials.

Some promising computational works are available in literature focusing both the stages. However, the studies are not coupled and not as developed as experimental works. A comparison between the numerical simulation and experimental observation is highly desirable, which is not usually observed in the literature. Moreover, the number of published works in the two-phase composite system is very limited. Therefore, relevant models for single-phase system are also discussed in this section that can potentially be applied for two-phase systems.

Thermal and fluid flow inside liquefier and nozzle

The models relating to the flow behavior inside liquefier and nozzle are some of the early works initiated by Yardmci,⁴² Rodriguez,⁴³ and Bellini.⁴⁴ The extrusion of single-phase polymer, the flow through the liquefier and nozzle, and the effect of nozzle geometry on melt swell were numerically studied. The pressure drop in the nozzle outlet, velocity, and temperature fields of the material and its effect on melt swelling and bead spreading was numerically modeled by Bellini.⁴⁴ In this work, the material behavior was considered as Newtonian assuming a 2D geometric profile. In recent times, Watanabe⁴⁵ performed similar work to investigate the temperature distribution, deposited bead shape, residual stresses, and deformation of fabricated parts with PC-based two-phase materials. The

2D flow behavior is also studied by Ramanath et al.,³³ where the flow field, temperature field, pressure gradients, and the effects of nozzle geometry were simulated. Later, the results were compared with an analytical model originally presented in Bellini's work. In a separate study, Mostafa et al.⁴⁶ simulated the same parameters with ABS/iron composite in a 3D domain. All these above stated works considered a constant liquefier wall temperature or constant heat flux for the entire heating assembly however, Stewart et al.⁴⁷ have presented a realistic 3D model with all the metallic assemblies in a FFF process and proposed a heat transfer mechanism considering external convection and radiative heat losses as shown in Figure 2. The model presented a gradual thermal evolution on PLA material due to the non-isothermal heating and compared with the experimentally measured temperature data at different liquefier-zones.

A similar 3D model has been developed by Papon et al.⁴⁸ with CNF/PLA non-Newtonian fluid, where the effect of nozzle outlet geometry on pressure drop, velocity, and temperature profile was investigated. Kim et al.⁴⁹ also developed a similar model with different nozzle geometries (circular, flat) for photo-curable thermoset polymer nanocomposite. The model showed different fluidic behavior with the changes in nozzle shapes at the nozzle exit. Recently, Osswald et al.⁵⁰ have developed an analytical model of melting behavior inside the nozzle considering the initial filament temperature, heater temperature, applied force, nozzle tip angle, liquefier diameter, and rheological and thermal properties of the materials. The model was able to predict the melting behavior at forces up to 40 N, but the melting rate was overpredicted at higher applied forces. However, these works lack the prediction of the fiber distribution and orientation once the melt is deposited.

Fiber orientation and flow field outside the nozzle

A very few works have been reported focusing on the fiber orientation in the FFF process. Among these studies, various parameters like the nozzle angle, fiber content, flow rate, and pressure difference were investigated, and its effects on fiber orientation and mechanical properties were estimated. Computational modeling has been performed using different commercial software like Moldflow®, ANSYS®, and COMSOL®. In two of the similar studies by Nixon et al.⁵¹ and Garcia,⁵² the effects of nozzle divergence, convergence and a straight channel with different material flow rate were investigated in Moldflow®. The nozzle designs were analyzed as axis-symmetric 2D cross-section using modified Flogar-Tucker equations.⁵³ The fiber orientation was described by analyzing the variation of orientation tensor along

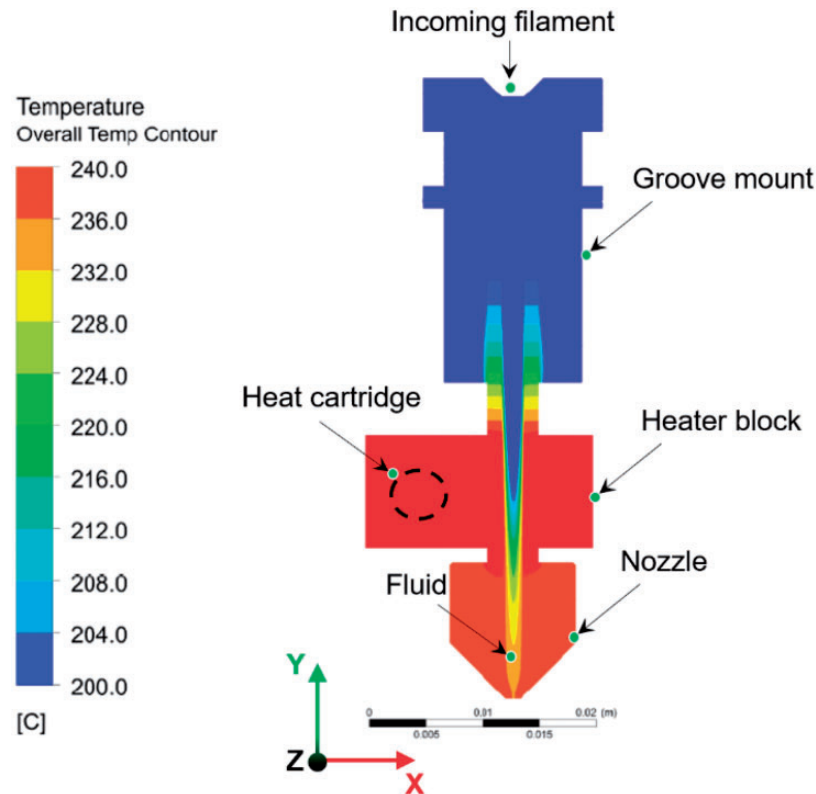


Figure 2. Liquefier, nozzle, and inside-fluid temperature profile⁴⁷ illustrating a temperature evolution throughout the liquefier channel and even temperature at the nozzle outlet.

Source: reproduced with permission from ASME, 2015.⁴⁷

the flow. The convergent nozzle yielded an increase in fiber orientation along the flow direction as compared to the conventional circular-exit nozzle. However, the divergent nozzle was found to decrease the fiber alignment. Based on the orientation tensor, an insight into the effects of these nozzle geometries on tensile moduli was also presented. An increase in nozzle divergence was found to decrease the first principal tensile modulus in simulation. Garcia⁵² extended the 2D model of Nixon et al.⁵¹ to a 3D domain and the 3D random fiber orientation was calculated to achieve mechanically isotropic extruded bead. However, the experimental investigation of these geometries are yet to be examined, and none of these studies considered the melt swelling effect. Later on, Heller et al.³⁴ modeled the fiber orientation, where the effect of melt swelling of carbon fiber reinforced ABS composite was considered, and the simulation was run in COMSOL[®] multi-physics with MATLAB[®] interfacing. The melt was assumed to be a Newtonian fluid, and the flow was modeled as incompressible (creeping flow). The nozzle shape, convergence zone, melt swelling, and its effects on the fiber orientation were the goal of these studies. The orientation tensor model by Advani and Tucker⁵⁴ and the isotropic rotary diffusion model from Floger-Tucker were used to

explain the fiber orientation. The results were almost similar to Nixon et al. and Garcia, with the exception of the effect of melt swelling. The effects of free surface expansion due to melt swell substantially decreased the fiber orientation. Thus, the decrease in fiber orientation also decreased the axial modulus of elasticity by about 20% and an increase in the radial modulus of elasticity by 6.62%. It was also observed that a change in the nozzle convergence length (A) and nozzle expansion length (D) have little effect on fiber alignment and mechanical properties. However, the straight tube portion (B) of the nozzle and nozzle diameter (C) were shown to have greater effect on fiber orientation. From a parametric study, the authors optimized the geometry for highest achievable elastic modulus in the bead-printing direction. The evolution of fiber alignment in the flow direction for the optimized geometry is presented in Figure 3.

In another publication,³⁴ the authors performed the finite element analysis of a 2D Stokes flow to evaluate large-scale extrusion system and computed the fiber orientation and its resulting mechanical properties of the CF/ABS composite. However, the study reported that a coupled fiber orientation and flow velocity model would improve the current results. In another

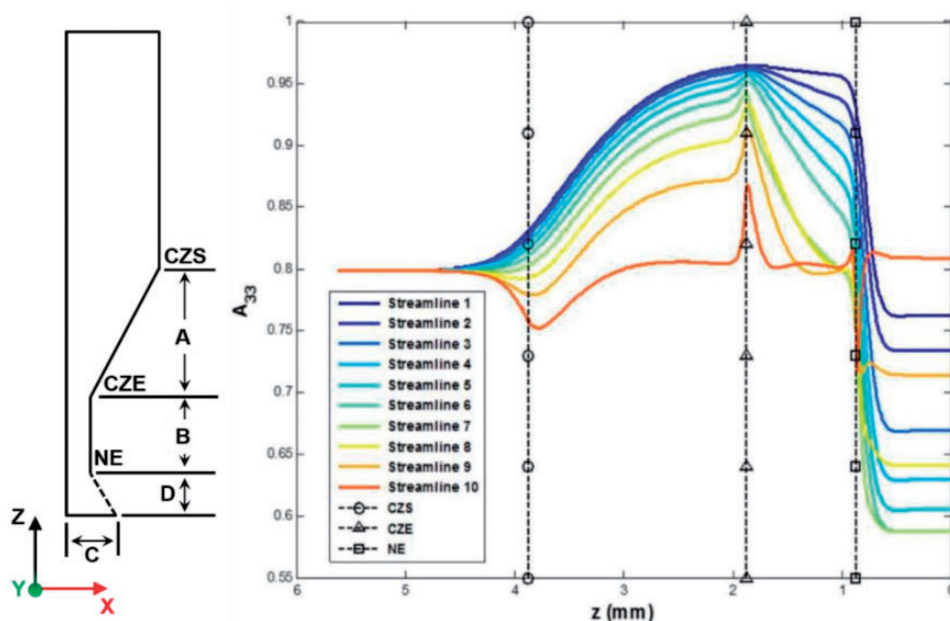


Figure 3. Modeling geometry and fiber alignment in the bead-flow direction at different z -distances of the nozzle.³⁴ The A_{33} components of the streamlines shown in the figure replicate the different orientation state encountered throughout the entire fluid domain.

Source: reproduced with permission from Elsevier, 2016.

CZE: End of convergence zone; CZS: Start of convergence zone; NE: Nozzle exit.

publication on the large-scale system by the same group,⁵⁵ the viscous effect of the material through Newtonian, generalized Newtonian, and viscoelastic rheology models were conducted, and the results of the obtained fiber orientation were compared. For large-scale pellet-based extrusion system in LSAM (like BAAM), the effects of single screw swirling motion in the melt flow and fiber orientation were investigated⁵⁶ (the reader is suggested to refer to the original article for modeling details). The results indicated that the swirling motion of the flow had a direct effect on fiber orientation, distribution, and associated average elastic properties of the CF/ABS bead. Lewicki et al.⁵⁷ modeled the flow field and fiber orientation behavior of CF/epoxy where the fiber–fiber, fiber–matrix, and fiber–wall interactions were considered. The fibers were modeled as separate, discrete particles and the fluids as an incompressible rigid body. The calculation started with the assumption of a random fiber alignment inside the filament, and the model predicted a gradual fiber alignment in the 3D domain under a simulated printing conditions. A realistic extrusion head was considered with circular nozzle-exit geometry. The simulation predicted a wall dominated shear alignment meaning higher fiber orientation close to the wall, then progressed inward towards the center following a parabolic velocity profile (as predicted by the fellow researchers discussed above). However, this

model as well as all other previous models computed the fiber orientation inside the nozzle or the melt adjacent to the nozzle.

Several studies have investigated the fiber orientation of the deposited bead on the print platform. Bertevas et al.⁵⁸ is one of the pioneers to model the fiber behavior on the deposited bead. A microstructure-based fiber suspension model coupled with a constitutive model for suspending polymer was implemented within the smoothed particle hydrodynamics (SPH) framework. The main goal of the work was to examine the effects of fiber aspect ratio (which was absent in other articles), fiber content, and the bead deposition speed. The results of fiber alignment at the nozzle was almost identical as reported by Lewicki et al.⁵⁷ However, a significant variation in orientation was observed between the nozzle and the deposited bead, suggesting that the fiber orientation at the nozzle should not be taken as an estimate for the fiber orientation in the printed bead. Moreover, the fluid viscosity, printing head internal angle, initial fiber orientation inside the nozzle were found to have a very insignificant effect on bead-fiber alignment. However, the fiber orientation on the bead was found to be highly sensitive to the printing process parameters. A similar observation is reported by Yang et al.⁵⁹ where the orientation characteristics were simulated for both the discontinuous and continuous CF/ABS composite. The modeling approach was based on the coupling

between SPH and discrete element method (similar to Bertevas et al.⁵⁸) having the flexibility to deal with free surface flow, large deformation of fibers, and fiber–fiber interaction which are relevant to the realistic FFF process. The orientation response of the short fibers were in well-agreement with the results presented by Bertevas et al.⁵⁸ The transient flow pattern of short and CFRPs at different time intervals are shown in Figure 4. Assuming a random fiber distribution and orientation as perpendicular to the flow direction, the fibers tend to highly align along the flow direction as the time progresses. At the nozzle exit section, the orientation is higher as seen from the flow profile at $t = 0.1$ s, which is also supported by previous literature.^{60–62} For the continuous fiber reinforcement, the fibers were firmly hold in the middle of the printing head due to the geometric symmetry as seen from the flow profile at $t = 0.05$ s. At $t = 0.1$ s, the fibers showed large bending deformation and a continuous-direct contact between fibers and nozzle edge, which might cause fiber breaking and the potential wear of printing head. Thus, especially for

continuous fibers, printing at a slower speed may be beneficial and reduce such fiber degradation tendencies.

The presented works on modeling the flow of fiber-containing polymers gives an insight of the fiber dispersion and orientation. There have been a few notable works along that line to experimentally observe the characteristics of fibers inside the nozzle and quantify the fiber orientation inside the nozzle and on a fully solidified printed bead. One such work by Yunus et al.⁴⁰ investigated the effects of shear rate and frequency on fiber alignment in the 3D extrusion process. The alignment was calculated in terms of orientation-tensor, and the results showed an approximate increase in tensile strength by 28% with the alignment of nanofibers. As a continuation, Yunus et al.⁴¹ later investigated the short fiber reinforcement on flexural properties. The results yielded an increase in flexural strength by $\sim 90\%$ with aligned CFs as compared to randomly oriented CFs and by $\sim 333\%$ compared to unreinforced samples. However, the article did not present any quantitative data of approximate fiber

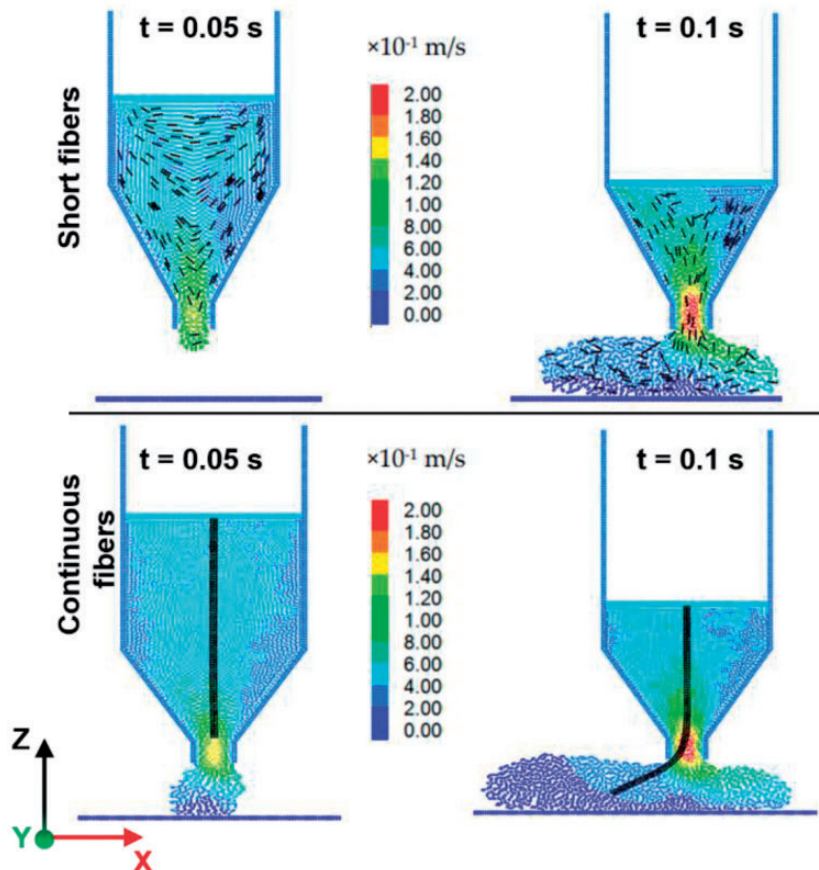


Figure 4. Velocity profile and fiber orientation evolution of short and continuous fibers.⁵⁹ The fibers were modeled as discrete particles, and fiber–fiber interaction was considered.

Source: reproduced with permission from MDPI, 2017.

alignment. In a recent study by Mulholland et al.,⁶³ the orientation in the bead was measured using micro-computed tomography. The results showed the orientation-tensor in the printed bead along the principal flow direction, a_{11} was about 0.65. The orientation-tensor in other two principal directions were lower and was approximated as a_{22} to be 0.20 and a_{33} as 0.15, respectively. A similar approach to quantify the fiber orientation for large-scale manufacturing system was conducted by Russel et al.⁶⁴ and Heller et al.⁶⁰ in separate studies.

Free space bead spreading and analysis of bead shape

The FFF-AM process is a complex, multi-step, and multi-physics phenomena. Once the melt is extruded through the nozzle, the next step is to deposit the bead on the platform and investigate its thermo-mechanical behavior, solidification, shape change, and crystallinity. The computational cost at this simulation stage is significantly higher than simulating the behavior inside the nozzle. The addition of fibers or any discrete particle makes the problem even more complex. Not many computational works have been conducted so far on the bead spreading and solidification process. Thus, a lot of the works presented in this section describing the bead spreading of unreinforced, single phase polymers.

Bellini⁴⁴ was one of the first authors to study the material deposition process of the FFF technique. A 2D planer flow model was developed in ANSYS®-Polyflow, and the fluid flow and heat transfer characteristic during the deposition of ceramic beads were studied. A similar 2D planar flow model was simulated by Watanabe⁴⁵ on polymers, and both these simulation results yielded similar trend of heat and flow

evolution on the deposited beads. They both further studied the deposition of multiple beads, however, Watanabe expanded the model to study the warping characteristics of polymers too. In these models, a constant nozzle wall temperature was assumed for computational simplicity, and the nozzle was maintained in a fixed position while the platform was translated in the horizontal direction with a constant velocity to simulate the relative motion between the nozzle and print platform. The similar “fixed-nozzle and moving-platform” strategy are followed in a lot of the consecutive studies by various researchers. Verma and coworkers⁶⁵ used Flow-3D® to simulate the deposition of three successive beads on top of each other by solving the Navier-Stokes, incompressibility, and heat-transfer equations. The model was coupled with the VOF method to track the free surface expansion with an assumption of Newtonian-fluid material model. Unfortunately, these studies lack experimental investigation of temperature and flow evolutions while printing. The real-time experimental data can give confidence in the numerical model. In a separate experimental study, infrared thermography based experimental measurement of temperature evolution was taken as a function of time. Figure 5 shows the comparison of experimental results and numerical simulations by Fitzharris et al.³⁷ The measurement of temperature rise due to the diffusion of thermal energy is found to be in good agreement with the simulated model.

In a recent study, Xia et al.⁶⁷ concentrated on the effects of melt viscosity and non-Newtonian melt behavior and presented a fully resolved numerical model of bead deposition on the heated platform and its gradual solidification. The model used a finite volume/front tracking method where the conservation equations for mass and momentum were solved on a

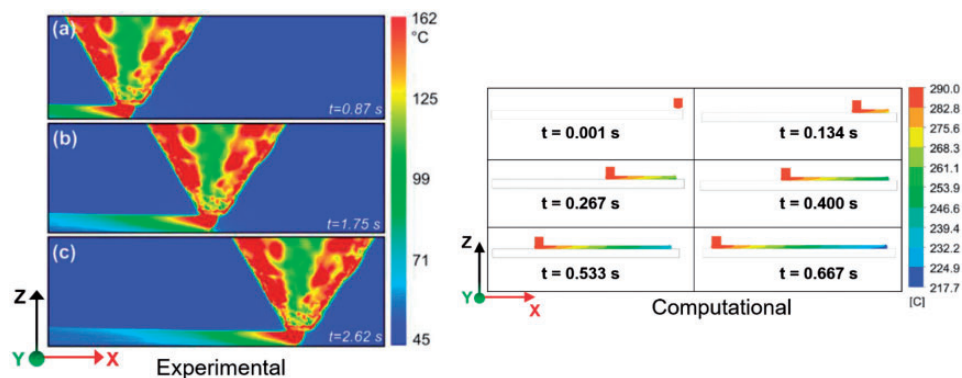


Figure 5. Comparison of experimental and computational temperature thermal analysis of bead, Experimental⁶⁶: infrared thermographs obtained at three different times for single bead spreading wherein the nozzle moves from left to right and Computational³⁷: temperature evolution and bead cooling wherein the nozzle moves from right to left.

Source: reproduced with permission from Elsevier, 2019 and Springer, 2017.

fixed, structured, and staggered grid. The fluid domain of different beads was discretized, and the bead-bead interface was tracked using connected marker particles. The non-Newtonian material model was introduced as a function of temperature and shear rate, and the nozzle was modeled as a volume source. The extrusion of melt was performed on a rectangular domain initially containing air, and both the air and melt flow behavior were simulated collectively. Later, the model was also able to simulate a complex, two-layer in-filled rectangular geometry. The study successfully predicted the shape of the bead, temperature distribution, contact area between the beads and the reheat regions of the deposited beads.

In a simplified bead spreading work, Comminal et al.⁶⁸ studied the dependence of bead shape on the distance (from the nozzle to platform) and the velocity ratio (between the platform translational velocity and average velocity of the flow inside nozzle). Newtonian-fluid material model and isothermal heating were assumed to simplify the model. The free surface evolution of the bead was captured by an algebraic coupled level-set (LS)/VOF method. The transport of field variables was computed by tracking the position of the surface. Interestingly, the results showed that the shear thinning behavior (Newtonian/non-Newtonian fluid) of the material have a very negligible effect on the bead cross-sectional shape. According to the model, the extruded bead was subjected to only the gravitational force, which was negligible to cause any deformation of the bead. The bead cross-sectional shapes were tailored only by varying the gap distance between the platform and nozzle. The results of the modeled cross-sectional shapes were compared with experiments, and a good agreement was established⁶⁹ between simulation and experiment, as shown in Figure 6.

In a successive publication, Serdeczny et al.⁷⁰ focused on the spreading of multiple beads on top of each other and side by side to investigate the effects of bead cross-sectional shape on inter-bead voids. The effect of layer thickness and bead to bead distance were studied, and the numerical results yielded that the inter-bead void is reduced with the decrease in bead to bead distance. However, the gap distance between nozzle and platform was not included (as presented in their previous work⁶⁹), and the simulation was run each as a complete simulation; one bead at a time. The same research group also presented another model to study the variation of bead width along the deposition direction. Different deposition strategies (sharp turning, smooth turning) were studied and an insight to over deposition and under deposition while nozzle-turning was presented.⁷¹ The modeling works were still in their early stages during the time this article

was written. However, it is worth studying the combined model in a single run. Moreover, the effects of the contact between the nozzle and extruded molten bead may also be included. For FRC (both continuous and discontinuous), the fiber-nozzle contact may cause fiber wear and tear as discussed in previously (Figure 4), which is also a potential area to study.

Balani et al.^{72,73} recently modeled the melt flow behavior in between the nozzle outlet and print platform (the gap distance, as mentioned by Serdeczny et al.⁷⁰). The rheological behavior of the melt (viscosity, shear rate) was given special attention in this study. The numerical model was simulated using the two-phase flow in COMSOL[®] multi-physics software. The LS and Navier-Stokes equations were used to determine the rheological properties of the flow with time. The results showed that at higher inlet velocities and shear rates, the flow shows instability, degradation, and the formation of uneven surfaces. The similar was observed for higher shear rates and higher temperatures. Such instability and degradation were reduced through optimization of temperature, nozzle diameter, and shear rate. However, the model did not present any heat transfer and bead spreading strategies.

The dynamic meshing capability is important to simulate the actual nozzle movement in FFF, which is not possible in any currently existing software. Liu et al.⁷⁴ have developed a viscoelastic multi-phase solver with the capacity for dynamic meshing to model the FFF nozzle-extrusion using OpenFOAM[®]. This model also considers the multi-phase flow when the fluid is in direct contact with air and print platform. The free surface-flow was modeled by VOF methodology. A solid body motion function was used to model the mesh transformation without deformation and dynamic motion solver to assign specific boundaries that are expected to move. Few parametric studies like the effect of nozzle geometry, printing temperature, and the time difference between bead-deposition were also conducted.⁷⁴ The results showed that a rectangular nozzle geometry with sufficient pause time and relatively lower print temperature (in this case, HDPE), a good bead spreading and good bead to bead bonding could be achieved.

Thermal history and bead solidification

The solidification of the deposited beads is an important factor for the bond formation between the adjacent beads. The overall mechanical behavior of the printed part is also largely dependent on such bonding. Thus, the models relating to the solidification process, crystallization, thermal history of the beads, and bead to bead bonding are discussed in this section.

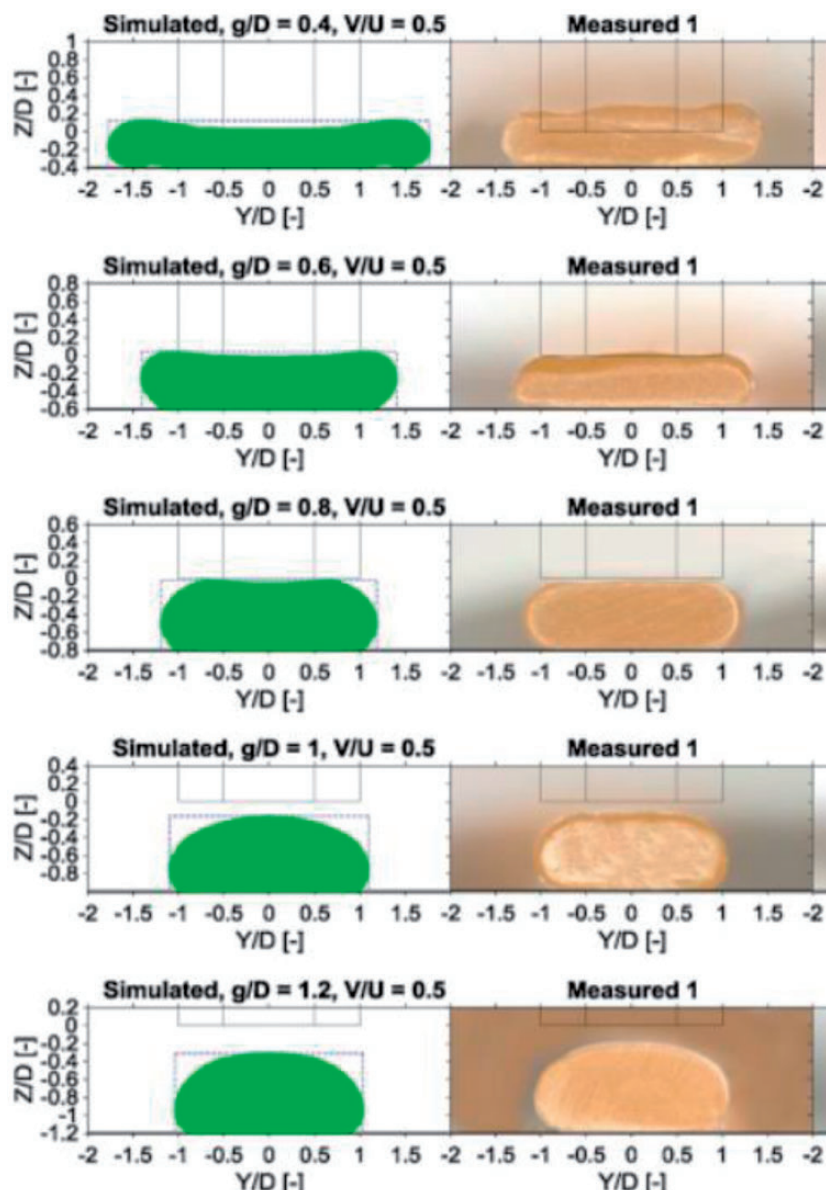


Figure 6. Simulated and measured cross-sectional shapes of the bead for platform velocity to inflow velocity ratio of 0.5 for different gap ratio (distance between platform and nozzle/nozzle diameter).⁶⁹ The black lines represent the nozzle geometry and position. Source: reproduced with permission from Elsevier, 2018.

These studies are mostly conducted on unreinforced materials.

Atif Yardimci et al.⁷⁵ published one of the first 2D heat transfer models of bead-bonding. Interactions with the surrounding environment and adjacent beads were modeled by including evolving heat sink terms. Convective boundary conditions were applied for simulating the outer edges of the beads. The effects of different Peclet and Biot numbers on temperature distribution were investigated. A similar 2D heat transfer model with rectangular cross-sectional beads was also investigated by Rodriguez.⁴³ In recent times, a simple 2D heat transfer model was developed by Brenken

et al.⁷⁶ applicable for fiber-reinforced system. The model is developed in COMSOL[®] multi-physics by coupling a non-isothermal dual crystallization kinetics model to understand the crystallization behavior during solidification. Stepwise activation of bead cross-sections was applied, and its thermal history and crystallization states were predicted. In this study, the temperature gradient along the deposition direction was assumed to be negligible, which may not be a very good approximation for a realistic case. However, a complete solidification cycle for a three-dimensional case is needed for better understating of the cooling process.

Zhou et al.⁷⁷ developed a simplified 3D bead-model in ANSYS[®] with a rectangular cross-section. Temperature-dependent heat transfer characteristics and heat capacity of the materials were incorporated in the model, and the printing process was simulated by a stepwise activation of the temperature profiles. Later, Pooladvand and Furlong⁷⁸ developed an analytical 3D heat transfer model by considering both convective and radiative heat losses. The temperature profiles from the numerical model were later compared with the experimental investigation. The earlier model by Brenken et al.⁷⁶ was also extended to a 3D state in ABAQUS[®]. The crystallization and re-melting of previously deposited beads were modeled with both convective and radiative heat losses. The model was able to predict the degree of crystallization of high-temperature fiber-reinforced PEEK and gave the insight to design the bead to bead bond-formation models.

It is well established that the orientation of polymer chains (crystallinity) have a significant effect on the properties of the final part. Thus, it is necessary to model the complex viscoelastic relations associated with stresses. Xia et al.⁷⁹ developed a viscoelastic bead deposition and solidification model like the ones presented by Liu et al.⁷⁴ The model included the evolution of the conformation tensor and the viscoelastic stresses. The numerical simulation was based on front-tracking/finite volume method, and the large variation in the material viscosity with temperature was solved using “implicit schemes” in the Navier-Stokes equation.

Figure 7 shows the shapes of the extruded bead, its temperature evolution, cooling, and deformation during the deposition of the second bead. The shape change and deformation are significantly different when comparing the effect of viscoelasticity. The viscoelastic stress caused much larger deformation, and the

tendency to deformation was higher in the regions where the shear rate was higher. The results also indicated that the viscoelastic stresses reduced the flow tendency of the melt and caused more accumulation of the material. Thus, it formed a thicker filament that caused the top of the filament to be squeezed harder on the bottom bead. However, the changes in polymer entanglement density (Rolie-Poly equation⁸⁰), entanglement losses, and inter-bead bonding were excluded from the study, which is worth investigating.

Aggressive efforts have recently been taken to apply the technology in making large-scale parts. Oak Ridge National Lab^{81,82} has been the leader of large-scale fiber-filled polymer-extrusion manufacturing. Similar efforts on medium-size extrusion are ongoing at Purdue University⁸³ and Baylor University.⁸⁴ Compton et al.⁸¹ have developed a 1D transient heat transfer model to analyze the temperature evolution and heat loss of a thin-walled polymeric structure in BAAM setup. The temperature in the through-thickness direction was assumed to be constant. Thus, the conduction was assumed only in the vertical direction. The model successfully predicted the bead by bead temperature evolution and gave an insight to the shape deformation tendencies during solidification. It was recommended to keep the bead temperature above the glass transition temperature of the material for reduced shape deformation and cracking. A separate work was published⁸² on the simulation of shape deformation and residual stresses of a full-sized car in BAAM which will be discussed in subsection “Residual stress and dimensional stability.”

Bond formation, crystallization, and bead-bonding

For the mechanical integrity of the printed part, bead to bead bonding and polymer crystallization is very

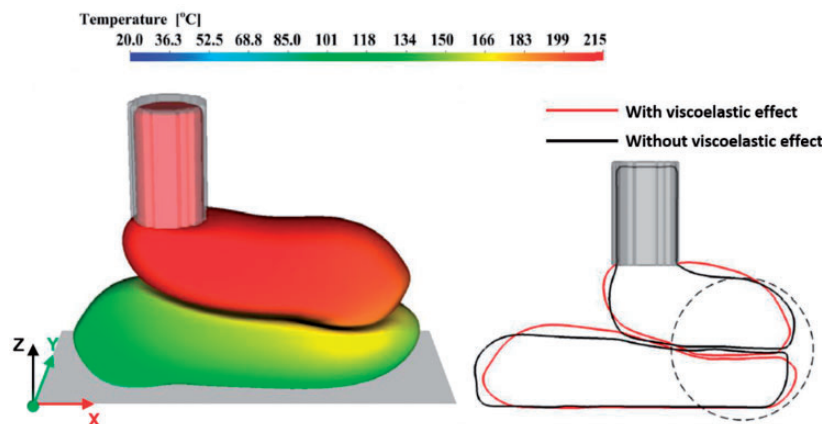


Figure 7. Comparison of the successive bead deposition, temperature evolution, and the effects of viscoelastic stress on bead shape deformation.⁷⁹

Source: reproduced with permission from Elsevier, 2019.

crucial. The crystallinity is important for the properties of the polymer, but the success of the FFF printed part mostly lies on the bead to bead bonding and molecular interactions at the bead interfaces. During the bead spreading and solidification process, two successive beads come in contact and start to form necking at their interface. The inter-diffusion of random polymer chains also takes place with time, thus creates an inter-bead welded zone. The quality of the bonding in terms of interface strength or toughness again depends on the FFF process parameters and polymer type (crystalline, semi-crystalline, amorphous, etc.).

Bellehumeur et al.⁸⁵ are one of the first authors to address the inter-bead bonding mechanism. They used a Newtonian polymer sintering model to create the neck formation between two adjacent beads and used a 1D lumped heat transfer model to predict the temperature evolution. Later, Sun⁸⁶ expanded the work by employing a non-isothermal diffusion model and predicted the degree of bonding. However, the model was reported to be very time and temperature sensitive. A later experimental investigation of molecular inter-diffusion by Shahriar et al.⁸⁷ showed a gradual neck growth mechanism and evolution of inter-diffusion for a semi-crystalline polymer, as shown in Figure 8.

In a separate work, Sun et al.⁸⁸ studied the effects of printing temperature and sintering temperature on thermal history and bond strength. The results showed a strong dependence of strength to sintering temperature. A similar correlation was later found by Gurrala et al.⁸⁹ where the spherical particle-sintering model was modified for cylindrical particle geometries.

Costa et al.^{90,91} developed another model for transient heat conduction during the bead deposition. The model considered the contact between adjacent beads, bead-platform, and also the heat transfer through the beads within the surrounding environment. Using a stepwise activation of the beads and a discretization of the geometry, a MATLAB[®] code was developed to predict the evolution of temperature and bead adhesion until the solidification process is complete. The model also considered the effects of FFF process parameters like the printing speed, bead dimensions, and bead material properties, sequence of deposition, and surrounding environment temperature.

In a series of publications, McIlroy et al.^{92–94} comprehensively studied the effects of polymer chains on crystallization. The models involved modified Rolie-Poly formula to account for flow-induced changes in polymer chain diffusion density and how the shear rate affects the polymer chain entanglement, crystallinity, and inter-bead chain diffusion. One of the papers⁹² showed that the degree of crystallization was increased with the increase in flow rate. The flow-induced crystallization increased the availability of spherulites to form chains across the bead interface that later fastened into crystalline structures on the bead-interface. This tendency increased the entanglement density and contributed to the resistance to the interfacial fracture. In a separate paper,⁹⁴ the flow-induced deformation and molecular chain interaction of amorphous polymers in FFF printing was modeled. In this study, the flow was assumed to be making a 90° turn to replicate the extrusion from the nozzle and subsequent spreading

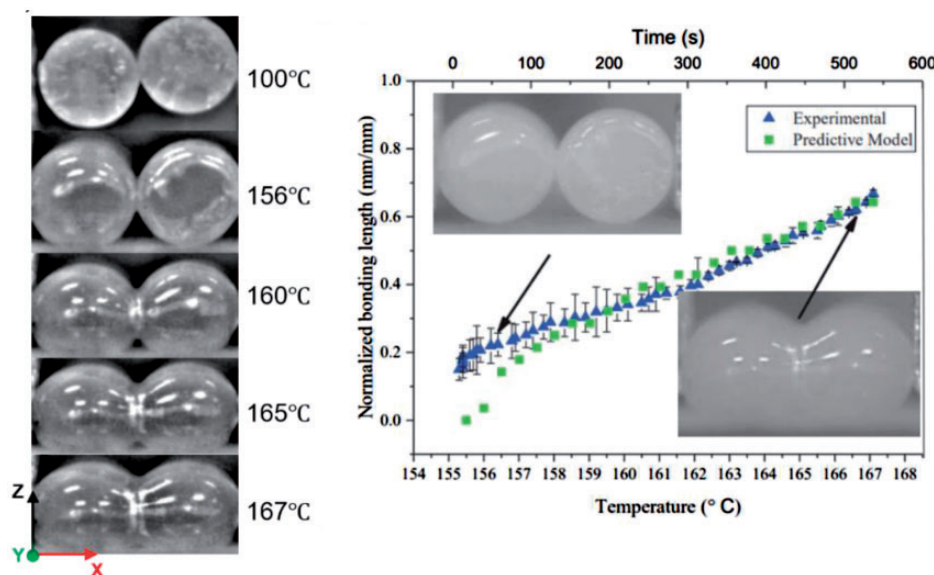


Figure 8. Experimental investigation of the gradual evolution of neck formation for semi-crystalline PLA.⁸⁷ Source: reproduced with permission from AIP Publishing, 2017.

on moving platform. The effects of different parameters like shear rate and convective constraint release on the molecular chain and deformation was studied. In succession, another paper by the same authors⁹³ presented a non-isothermal FFF inter-bead bonding model and the effects of printing temperature, printing speed, and molecular weight of the materials. One of the key findings of the work was to uncover the inter-bead bonding mechanism. The results showed that the key mechanism responsible for reduced mechanical strength at the interface is the initial disentanglement of molecular chains inside the nozzle and the delay in entanglement recovery due to the relaxation of the deposited beads. Figure 9 shows the relation between entanglement number and bead-interfacial fracture toughness, which was found highly sensitive to print temperature and print speed. The readers are suggested to refer to the original article for detail understanding of the relation between entanglement number, molecular weight, and fracture toughness.

Very recently, Barocio et al.⁹⁵ developed a model by coupling the bonding process of adjacent beads to predict the degree of bonding, temperature history, crystallization, and diffusion of semi-crystalline polymer chains. The coupling was implemented in UMATHT user subroutine in ABAQUS[®], and the degree of bonding was calculated through simulated beads of different layers with different cooling and crystallization rates.

However, the models were restricted for linear amorphous polymers only. Usually, amorphous polymers are widely used with FFF due to their low shrinkage while solidification. However, different available FFF-printable materials have different characteristics like ABS is an amorphous polymer, PLA without any filler behaves like an amorphous material, but with tricalcium phosphate behaves like a semi-crystalline

polymer,⁹⁶ polybutylene terephthalate, polyamide 12 (PA 12), PEEK are semi-crystalline^{97–99} in nature. The effects of different reinforcement on these polymers in terms of viscoelasticity, printing quality, and shrinkage while solidification are worth investigating.

Residual stress and dimensional stability

The residual stresses induced in the beads during the printing process affect part strength and shape deformation. This section would describe a few of the notable modeling strategies adopted so far to address the dimensional accuracy and formation of residual stresses.

Wang et al.¹⁰⁰ was one of the first authors to address the part deformation after printing and established a simplified analytical model with rigorous assumptions and simplifications. However, the model was good to provide an insight into the bead deposition strategies (tool path) that could potentially limit the formation of residual stresses. Xinhua et al.¹⁰¹ developed a 2D model based on the elasticity theory of thin plates (equilibrium, Hook's law, and strain displacement relationships). However, this model was also simplified with the assumption that there were no thermal stresses between the glass transition temperature and the melt temperature of the material, and the beads were deposited instantaneously. Very recently, Wijnen et al.¹⁰² presented a modified Wang et al. model by replacing the temperature step function (Wang et al.¹⁰⁰) with a physics-based temperature gradient. The three components of temperature in this work were conductivity, convection, and radiation. The model was able to predict the distortion behavior successfully, but there was a limitation in terms of predicting the magnitude of deformation. Armillotta et al.¹⁰³ presented a separate analytical model considering both the elastic and plastic behavior of single and multiple layer shrinkages due to the formation of residual stresses. The authors observed that the residual stress, shrinkage, and surface roughness were increased greatly with the increase in layer thickness.

In a 2D model by Fitzharris et al.,³⁷ a parametric study was conducted on the residual stress behavior by changing the material properties in ANSYS[®]. The model was a coupled Polyflow-Mechanical analyzer to model the bead flow, solidification, and subsequent structural simulation to examine the residual stresses. The coefficient of thermal expansion (CTE) of the material was found to be highly significant for controlling the residual stress than the heat capacity, thermal conductivity, and elastic modulus of the material. For reinforced (carbon, graphene, CNTs, etc.) material system, the CTE can be highly tailored which can reduce the formation of residual stress, part warpage, and shrinkage. However, the numerical model used in

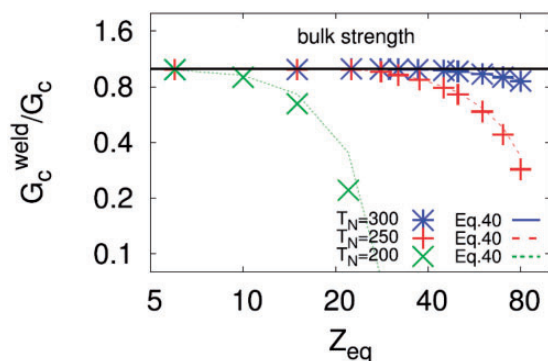


Figure 9. Log-log plot of the bead-interfacial fracture toughness at the interface zone G_C^w normalized by the equilibrium fracture toughness G_C for a fixed print speed of 10 mm/s and three print temperatures $T_N = 200, 250$ and 300°C where Z_{eq} represents the equilibrium entanglement number.⁹³

Source: reproduced with permission from Elsevier, 2017.

this study was not a single-continuous simulation, rather a combination of multiple simulations. The results of one model were transferred to another model. A complete 3D numerical model would best represent the actual physical scenario.

Zhang and Chou^{104,105} described the onset of thermal stresses as a time-dependent phenomenon in a 3D FEA model. It followed the speed of nozzle movement along the bead-deposition path and considered both radiative and conductive heat losses. The coupled equilibrium and energy conservation equations were solved as an iterative process in ANSYS[®] and calculated the 3D residual stress fields. However, the model was considered as a solid body neglecting the bead-bead interfacial interaction. The results were later compared with the experimental tests by varying different FFF process parameters like print speed, bead and layer thickness, and its effects on the final part deformation. The authors reported the printing speed to be the critical parameter for generating residual stresses. However, no further works on the quantification of deformation were published by the authors.

Xia et al.¹⁰⁶ extended their initial 3D melt flow model⁶⁷ adding a more realistic nozzle simulation. They used an immersed boundary to represent the

cylindrical nozzle channel, and the melt was assumed to be extruded through the channel. A material deformation model was also added to capture the deformation gradient with time. Also, a separate material model was added to account for the polymer-bead shrinkage as solidification proceeds.

Figure 10 shows the temperature and mean stress plots at different times, representing the evolution of temperature and residual stresses in the beads. The higher stresses at the end of the beads were the results of linear shrinkage in the longitudinal direction due to the higher temperature gradient. The large temperature gradients were likely to contribute to the residual stresses of the beads. However, the effect of platform temperature was not accounted for this simulation, which might yield interesting findings on the same characteristics. In a recent study by Xia et al.,¹⁰⁷ the shape of the deposited bead was studied using a front tracking method.

Du et al.¹⁰⁸ also simulated a 3D bead spreading model with external heating to address the warping, deformation, and cracking during large-sized thin-walled parts. The numerical model was based on the semi-implicit pressure linked equation algorithm. The VOF method was used with piecewise linear

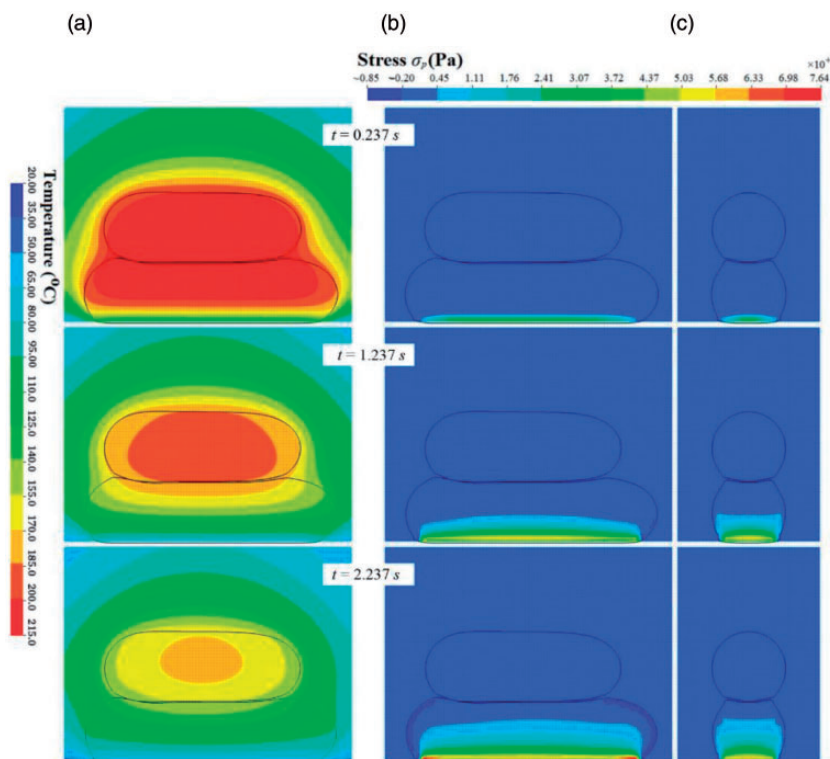


Figure 10. The temperature and mean stress plots at different times, (a) temperature at three times in a longitudinal cross-section through the middle of the domain, (b) mean stress in the same plane, and (c) mean stress in a perpendicular plane cutting through the middle of the bead.¹⁰⁶

Source: reproduced with permission from Emerald Publishing Ltd, 2018.

interface construction to reconstruct the free surface, and the classical Navier-Stokes and energy equation were solved for capturing the dynamic flow field inside the bead. In this work, the dependence of viscosity on temperature and shear rate was considered, and the melt was modeled to be a non-Newtonian fluid.

In a recent study, Cattenone et al.¹⁰⁹ presented a 3D-FEA-simulation framework in ABAQUS[®] to perform the part deformation analysis through sequential element activation as used by previous few works. The influence of simulation parameters like the time-step and meshing was analyzed with temperature-dependent mechanical properties. The model was able to capture the deformed shape with an acceptable agreement with the experiment. However, it did not introduce any adhesion model to address the interaction between the beads and print platform.

Favaloro et al.⁸³ are one of the first to present a model to understand residual stresses and resulting deformation of a 50 wt. % carbon fiber filled PPS composite part. The model was developed in ABAQUS[®] through the progressive element activation method as already discussed in Brenken et al.⁷⁶ work. A 3D heat transfer and crystallization model was coupled with the residual stress model. The shrinkage due to material crystallization, the deformation due to residual stresses, and additional deformation while removing the part from the build platform were analyzed on a complete air inlet duct tool.

A comprehensive full-scale car model made of 3D-printed composites was first published by Talagani et al.⁸² from ORNL. A coupled thermo-mechanical FEA model was developed, and sequential element activation was used to simulate the bead-deposition process. The orthotropic material properties of the composite were assigned based on the bead orientations. The goal of the simulation was to identify potential stress-concentration areas where the layer-delamination might occur by using the linear elastic fracture mechanics and

damage mechanics. The model predicted both the deformation due to thermal stresses and for residual stresses after solidification, as shown in Figure 11. The developed computational tool was also suggested to use to obtain a sensitivity of the process parameters.

Structure-property relationship of two-phase materials

Based on the physical understanding of the process, it is highly likely that the process would induce large variations in mechanical properties and anisotropy until and unless the intrinsic limitations are not resolved. This section provides the current state-of-the-art of structure-property relationship of reinforced thermoplastic polymers. Recent research attempts on improving the mechanical integrity in terms of strength and stiffness of the FFF-parts are summarized in three categories: nanoscale particles, micron-size discontinuous fibers, and continuous fiber reinforcement. The FFF manufacturing is driven the quality of the filament material and these filaments can be made using both single screw extruder and twin-screw extruders with different types of reinforcement in different thermoplastic materials. Thus, all the commercially available FFF 3D printers can be used to process nano and discontinuous FRC. For low temperature FRPCs ($\sim 250^\circ\text{C}$), few notable manufacturers are Stratasys[®], MakerBot[®], Ultimaker[®], Cincinnati Incorporated[®]. Companies like Stratasys[®], Intamsys[®], Cincinnati Incorporated[®], Tractus3D[®], Roboze[®], Apium[®] are mentionable for high-temperature ($>400^\circ\text{C}$) manufacturing capability. There are very few manufacturers on continuous fiber printing capabilities and Markforged[®], Anisoprint[®], Arevo[®] are few of them. The length of short carbon fibers (SCF) summarized in this section is in the range between 50 and 500 μm and diameter between 7 and 10 μm . If at least one of the dimensions of the reinforcement is in the nanoscale, those studies are grouped as

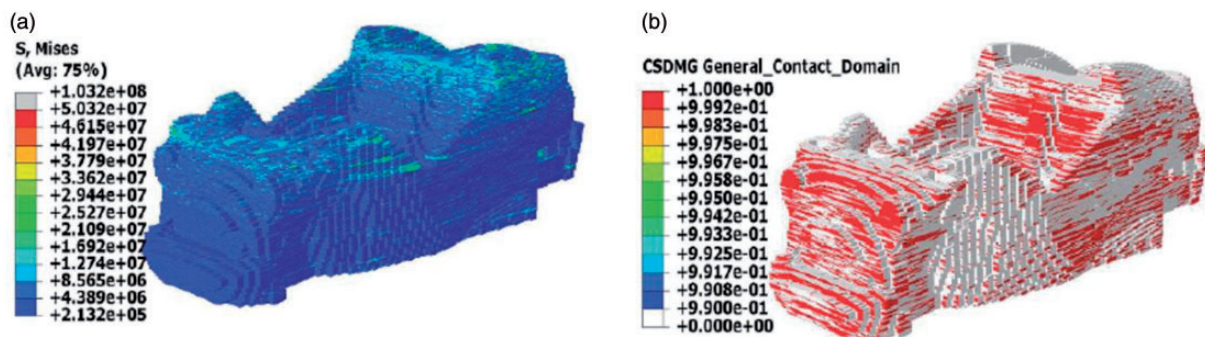


Figure 11. Simulation of a full-scale Strati car, (a) residual stresses due to process parameters after the part is printed and solidified, (b) crack initiation zones due to the thermally induced residual stresses.

Source: reproduced with permission from SAMPE Journal, 2015.

nanocomposites. The length and diameter (except GnPs) of the nanofibers discussed in section “Nanocomposite” are in the range of 0.4–2.5 μm and 9.5–50 nm, respectively. The mostly used matrix materials are found to be ABS and PLA with some works on PEEK, Ultem, PC, PA-12, etc. The majority of the published works attempted to improve the mechanical properties by comparing with the baseline polymer. A very few comparisons are made with the conventionally manufactured parts to understand the current standing of the FFF technology.

Nanocomposites

The most useful nano-reinforcements are found to be CNTs,^{110–118} CNF,¹¹⁹ GO,¹²⁰ xGnP,^{112,121,122} and nanoclays,¹²³ which are used with ABS, PLA, PEEK, PC, and PA12 polymers. Figure 12 summarizes the reported mechanical properties for different nanocomposites. It is to be noted that the data presented here is the maximum attainable from the respective literature (different nanoloading and different process parameters). The mechanical properties of the FFF-parts are the highest when the load is applied along the bead-printing direction.¹²⁴ Thus, Figure 12 includes only the summary of the in-plane directional properties. The reinforcing agents are highly aligned longitudinally along the bead deposition direction due to the shear flow. Typically, such orientation is represented in terms of orientation tensors. The orientation state in the bead printing direction referred to as a_{11} is reported

as discrete values of 0.68 and 0.8 for printed laminate and single bead, respectively.⁶³ The tensile strength and elastic modulus of the nanocomposites are the highest when the samples are loaded along the bead-printing direction as opposed to other orientations. However, the effects of other process parameters like the printing speed, solidification rate, layer thickness are not included in this section.

The majority of the summarized strength ranges between 20 and 50 MPa, while the elastic modulus lies between 1500 and 3000 MPa. It is found that the highest stiffness is achieved by Coppola et al.¹²³ with 4 wt. % clays/PLA composites. The elastic modulus was recorded to be 4423 MPa. However, the strength was not that promising. The highest strength (~ 80 MPa) for the two-phase CNT/PLA system was achieved by Lebedev et al.¹¹⁵ with 0.5 wt. % CNT content. In a separate study by Nadernezhad et al.,¹¹⁶ 1 wt. % CNT/PLA showed a significant increment in both strength and elastic modulus. The strength was recorded to be about 60 MPa and elastic modulus as 3950 MPa. A recent study by Gonçalves et al.¹¹⁷ showed promising increment in both strength and stiffness with high-temperature PEEK-based hybrid composite. The hybrid 3 wt. % CNT- 3 wt.% GnP/PEEK composite yielded the elastic modulus to be 3950 MPa and tensile strength as 93 MPa. In a separate study by Berretta et al.¹²⁵ on CNT/PEEK system revealed that the tensile strength is highly dependent on the nano-reinforcement loading. For 1 wt. % CNT, the system yielded highest strength whereas, 5 wt. % CNT loading

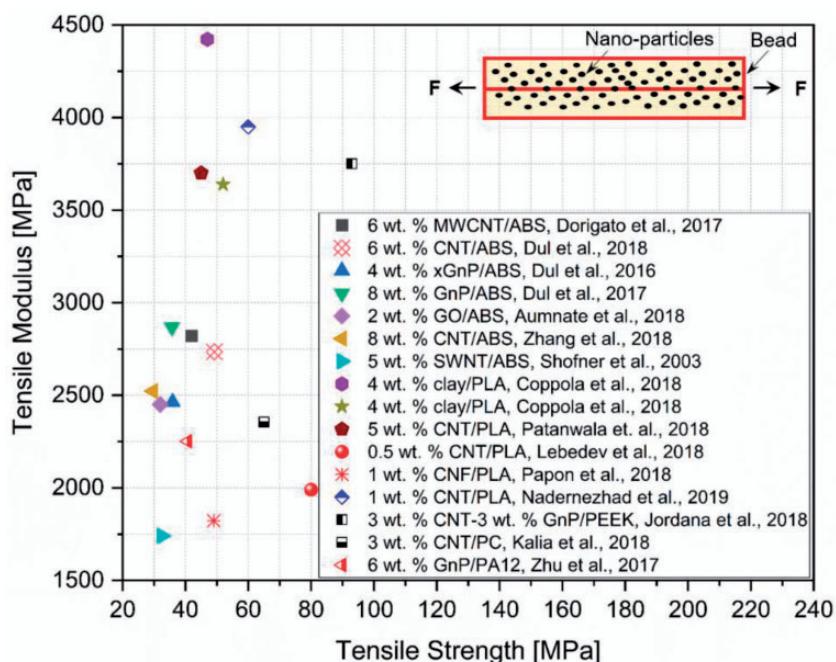


Figure 12. Tensile properties of FFF-printed nanocomposites,^{110–123} where the load was applied along the bead-printing direction.

showed a decrease in strength, being lower than the neat PEEK. A similar decrease in strength is also observed by Papon et al.¹¹⁹ with CNF/PLA nanocomposite. The 0.5 wt. % CNF loading showed highest increase in strength which again decreased for 1 wt. %. Higher amount of void contents were observed in these studies for higher nano-reinforcement, which shows the importance of interaction between the reinforcing agent and polymer matrix during the printing process. The lack of such interaction and fiber-matrix bonding induced voids and affected adversely on the mechanical properties. Despite the variability in strength and stiffness, the FFF-nanocomposite has a real promise in the nanotechnology. Multifunctional capabilities can be incorporated in a FFF-printed part by tailoring the nanostructure through controlled nanoreinforcement. The sensors industry can be benefitted using CNT, xGnP-based nanocomposites where higher degree of sensitivity and dynamic range can be achieved in a 3D printed sensor.¹²⁶

Discontinuous FRC

The mechanical properties of the discontinuous fiber-reinforced composites are studied largely in the open literature. The effects of different types of fibers and their content on strength and stiffness were focused on these published works. These studies were mostly conducted on ABS, PLA-based composites and a few with the high-performance polymers like PEEK, PEI, Ultem, TPU,

etc. Carbon fiber,^{8,61,62,113,127–136} vapor grown carbon fiber,^{110,137} jute,¹³⁸ glass fiber,^{61,139} kenaf bast fiber,¹³⁰ Hemp,¹⁴⁰ etc. were used as the reinforcing agents. It is to be noted that in some studies, the fibers were synthesized, and some were natural fibers. The readers are suggested to refer the original article for further details of the quality and characteristics of the reinforcing fibers. Figure 13 shows the summary of the tensile properties for the short FRC where the recorded data presents the maximum properties attained by each of the individual works. The tensile properties of the printing direction are presented in Figure 13. Thus, the fibers are also aligned along the same direction giving superior mechanical properties. The distribution and orientation of such short fibers are analyzed through optical microscopy and scanning electron microscopy by several types of research.^{62,129} The tensile strength mostly ranges from 10 to 75 MPa and the elastic modulus is mostly in the range of 1000–9000 MPa. A wide range of fiber contents was used, ranging from 4 to 50 wt. %. A significant difference in the trend of property improvement is observed for micron-sized, discontinuous fiber reinforcement in comparison to nanoreinforced composites. With the increase in CF content in CF/PA12 composite by Liao et al.,¹³⁴ both the modulus and strength increased linearly and the highest modulus and strength were achieved to be 3500 MPa and 90 MPa, respectively at 10 wt. % CF loading. However, for the GnP reinforcement by the same authors,¹²² the strength showed a

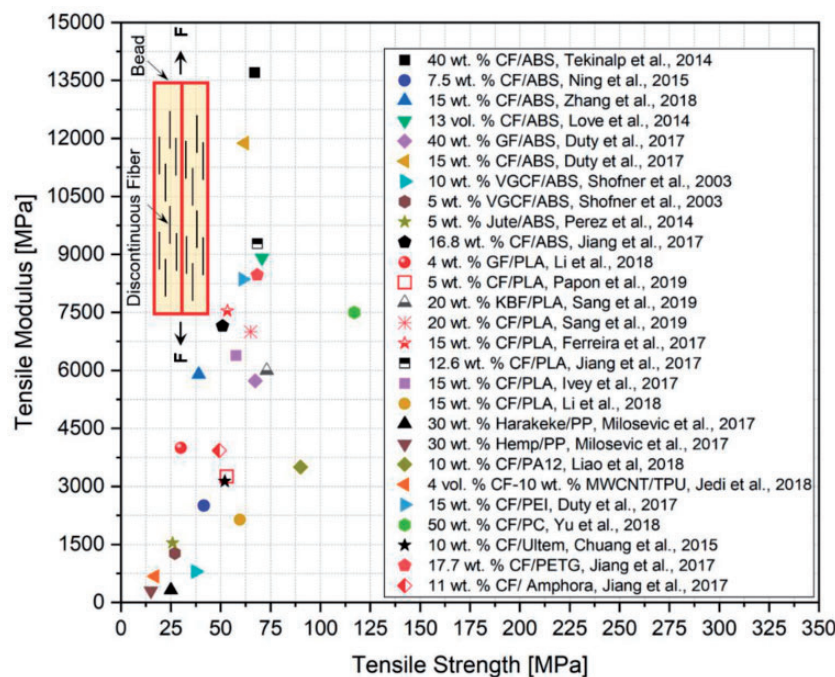


Figure 13. Tensile properties of FFF-printed discontinuous fiber reinforced polymer; summarized from^{8,61,62,110,113,127–140} where the load was applied along the bead-printing direction.

decreasing trend (40.7 MPa) with a slight increment in modulus (2251.7 MPa). The highest modulus of 13,700 MPa was achieved by Tekinalp et al.⁶² for 40 wt. % CF/ABS blends with the strength being 67 MPa. At the same fiber content, GF/ABS yielded similar strength response but the modulus was found to be less than half (5730 MPa) of what was achieved in the CF/ABS system. Furthermore, the same strength range is observed for different other material systems (CF/PLA, CF/PETG, and GF/ABS) with lower fiber contents (less than 20 wt. %) too. Interestingly, Duty et al.¹²⁷ reported a significant increment in both strength and modulus for BAAM setup at only 15 wt. % CF loading into ABS. However, the highest tensile strength reported so far is 117 MPa for 50 wt. % CF/PC composite by Yu et al.¹³⁵ This shows that the matrix material does not play a major role in maximum load-bearing capability rather it depends on the type and amount of fibers, fiber–matrix bonding, void contents, and process parameters, etc.

The presented data shows a wide variation in strength and stiffness. There can be several aspects of such variation. The fiber aspect ratio and the critical fiber length ($l_c = \frac{\sigma_{fu}}{2\tau_i} d_f$) largely affect the load transfer mechanism of the composite. Here, l_c is the critical fiber length, σ_{fu} is the ultimate fiber strength, and τ_i is the shear strength of the resin. As a result, with the same fiber content (10 wt. % CF loading) Tekinalp et al.⁶² (fiber length = 370 μm) observed higher strength (55

MPa) and modulus (8000 MPa) than Ning et al.⁸ (fiber length: 150 μm , strength: 35 MPa, modulus: 2200 MPa). Usually, the fiber breakage phenomenon is common too in the FFF-printing process during fiber–matrix blending and printing. Thus, a good number of fibers fail to pass the critical length requirement and may not take part in the functionality. Apart from that, the improper fiber–matrix interaction results in poor fiber–matrix bonding and creates micro-voids at their interfaces,^{8,62,141} reported by few investigations. These voids act as stress-concentration points and affect adversely under loading by failing the structure at a lower stress than expected.

Continuous FRC

Continuous fiber reinforcement in FFF-composites is the latest inclusion that tremendously expands the capabilities of FFF in structural applications. To the author's knowledge, Markforged^{®142} is one of the pioneering companies that has launched the FFF-printers capable of manufacturing continuous fiber-reinforced thermoplastic composites. Several research articles on CFR composites are published using Markforged[®] printer, and there are few works by custom-made CFR-FFF printers. A good number of articles are found on continuous CF, GF, KF-based nylon composites^{143–150} processed through Markforged[®] printer. Few independent works are found on PLA,^{151–155} ABS,^{156,157} PA,¹⁵⁸ and PEEK¹⁵⁹ based CFR

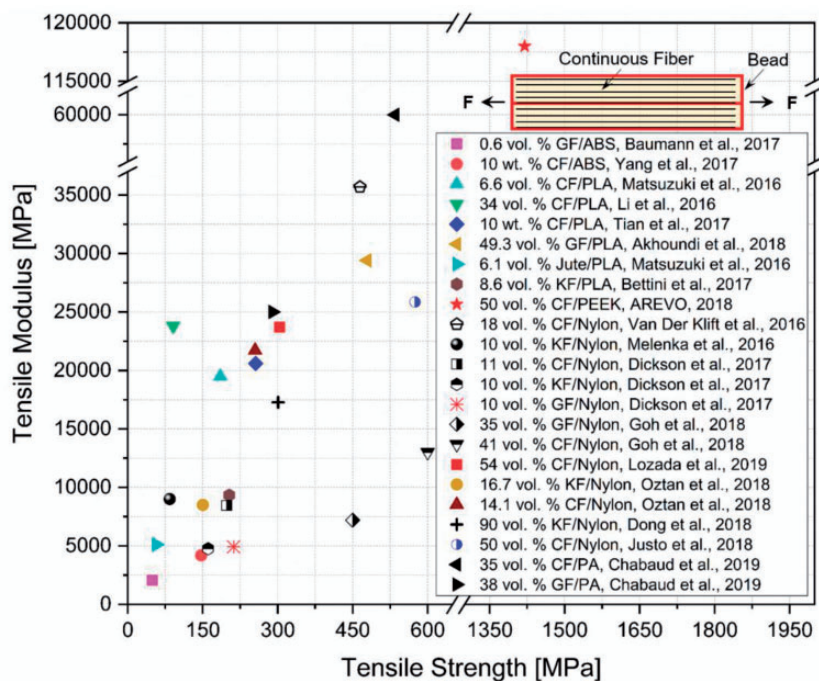


Figure 14. Tensile properties of FFF-printed CFRP composites,^{143–159} where the load was applied along the bead-printing direction.

composites. Figure 14 shows the summary of the tensile properties of CFR composites, where the recorded data presents the maximum properties attained by each of the individual works. Most of the data here are presented in terms of fiber volume fraction. The authors believe the reason maybe because of the Markforged[®] software's inherent capability to automatically calculate the fiber content in terms of volume fraction.

A wide range of mechanical properties is achieved with the CFR-system. The tensile strength mostly ranges from 50 MPa to 300 MPa and the modulus ranges from 2050 MPa to 25,000 MPa. The higher fiber contents are found to improve the mechanical properties significantly. It can be inferred from Figure 14 that fiber volume fraction above 30% shows significant improvement in both strength and modulus. The tensile strength crossed the 450 MPa mark for any fiber content above 30 vol. %. However, the elastic modulus was found to vary depending on the type of fibers. Generally, CFs showed the largest increment in modulus than GFs and KFs. However, in some studies, the GFs¹⁵⁴ were found to improve both modulus and strength than CFs¹⁴⁷ at a lower fiber content too. The highest modulus was reported to be 118,000 MPa with the tensile strength being 1412 MPa by AREVO^{®159} with 50 vol. % CF/PEEK using their custom-made printer. This is the only study found to date on aerospace-grade, high-quality polymer like PEEK. In a separate study by Chabaud et al.,¹⁵⁸ 35 vol. % CF was found to improve the properties greatly with PA matrix. It is found that the quality of the matrix material also plays a big role in improving the properties of CFR-systems. The highest fiber volume fraction used to be 90%, reported by Dong et al.¹⁴⁹ for the KF/Nylon system, however, the results did not yield any significant enhancement in properties. From the above summary, it is found that the CFR-system can very well reach or even exceed the strength of aerospace-grade aluminum¹⁶⁰ and in terms of stiffness, higher fiber content with a high-performance polymer like PEEK¹⁵⁹ showed promise to reach the stiffness margin too.

The summarized mechanical properties showed significant improvement in composites technology; however, the mechanical responses are still unpredictable due to its intrinsic limitations. The CFR-system significantly improved the properties in the loading direction, but the issues like bonding between fiber-matrix and bead-bead need serious attention to examine the part responses.

Future needs in FFF

Despite the promising aspects, the properties of the composites were found to vary significantly. The

bonding between the fibers and matrix is a big challenge along with the amount of reinforcement of short and nanofillers and nozzle clogging.⁶² Very recently, Nawafleh and Celik¹⁶¹ developed a vibration-assisted nozzle unclogging system for the direct-write AM system by adding multiple vibration motors to simultaneously shake the nozzle and extruder channels. This approach helped to avoid the material adhesion and fiber agglomeration and reduced fiber clogging significantly. The authors were able to print thermoset resin with 46 wt. % short fiber content, which is the highest reported short fiber-filled AM printing to date. The similar technology and/or redesigning the nozzle shape and through process parameters optimization, the nozzle clogging issues can be addressed for FFF-based AM too. The bonding between the fibers and matrix can be improved by proper surface treatment of the fibers before printing and improve the compatibility between the fiber and matrix. Comparing Figures 12 and 13, it is obviously seen that the fiber volume fraction used in different studies of discontinuous fiber composites are higher than those filled with nanoparticles. In AM and even in any conventional processing techniques of nanocomposites, dispersion of nanoparticles is a challenge, especially at higher particle loading. The weak interaction between polymers and nanoparticles typically leads to agglomeration and poor dispersion, which results in nonequilibrium effects and loss of interfacial area at high loadings.¹⁶² Along with this, the van der Waals attraction, effect of the surface area of nanofillers, π - π bonding between individual fillers, and dangling carbon bonds are also reported to be responsible for agglomeration.¹⁶³ Different modification techniques are adopted so far on conventional processing techniques for better dispersion of nanoparticles into the matrix as discussed by Uddin and Sun,¹⁶⁴ but none on AM of nanocomposites, to the knowledge of the authors. Different analytical models^{165,166} and molecular dynamic simulations¹⁶⁷ have been developed to investigate the effect of particle size, dispersion, and agglomeration on the interfacial/interphase properties and mechanical properties of the nanocomposites. In these studies, it is found that the agglomeration of nanoparticles weakens the positive attributes of the particles and significantly decreased the elastic modulus, whereas a fine dispersion produced a high modulus. This could be a potential field to explore for the large-scale screw-driven system, where a better control can be introduced into the fiber-matrix mixing chamber for better dispersion of particles. Along with this, another challenge in AM would be handling the potential nozzle-clogging at higher particle loading. Vibration-assisted nozzle unclogging system as discussed earlier¹⁶¹ or any

innovative technologies could be developed to address this issue.

Anisotropy in the transverse direction

One of the biggest challenges in FFF-AM is the anisotropy in material properties. The strength in the z-direction depends on the bead to bead bonding quality. Moreover, higher fiber loading weakens the bead to bead bonding, resulting in lower inter-laminar shear strength. A comparison of properties for FFF-composites in loading (x-axis) and transverse (z-axis) direction is presented in Figure 15. The presented data gives an overview of the responses for nano,^{113,138,168} micron,^{61,113,127,128,131,138} and continuous fiber¹⁵⁸ reinforced FFF composites. Some of the studies presented here are from large-scale systems too.

It is found that the reduction in strength and modulus for nanoscaled reinforcement is in the range of 25%–65% and 20%–30%, respectively. The tendency of reduced strength is very significant for short fiber reinforcement and becomes worst for continuous fiber reinforcement. The difference in tensile strength and modulus for short fiber reinforcement is in the range of 50%–93% and 44%–87%, respectively. The tendency of reduced strength and modulus even increases with higher fiber content. The CFR-system yielded a sparkling 97% reduced strength and modulus¹⁵⁸ in the z-direction than x-direction, which shows almost no

interfacial bonding (z-direction) present in the processed part. Therefore, although unidirectional-bead print orientation enhances the properties, the anisotropy in transverse direction tends to increase dramatically. Such anisotropy is highly dependent on the quality of the bead to bead bonding. This bonding is again a function of the thermal history and cooling profile of the deposited beads and directly affects the polymer coalescence mechanism. Tronvoll et al.¹⁶⁹ studied the effects of inter-bead voids on structural properties of single-phase FFF parts. Due to the change in thermal history between two adjacent beads (already deposited bead and newly deposited hot bead), the polymer diffusion through the bead interfaces remains incomplete and the corresponding cross-sectional areas get reduced and introduce inter-bead voids at the interface. In separate studies, these void shapes are found to be diamond and triangular shaped, depending on the bead cross-sectional shapes and bead deposition patterns.^{62,119} Tekinalp et al.⁶² explained the formation of such inter-bead voids in detail for two-phase composites. At lower fiber content (~0–10 wt. %) these are more dominant but at a higher fiber loading (~20–30 wt. %) they become lowered. Two reasons were explained for the reduction of voids at higher fiber content: decreased die swell due to the added carbon fibers resulting in smaller deposited beads and increased thermal conductivity. The increased thermal conductivity

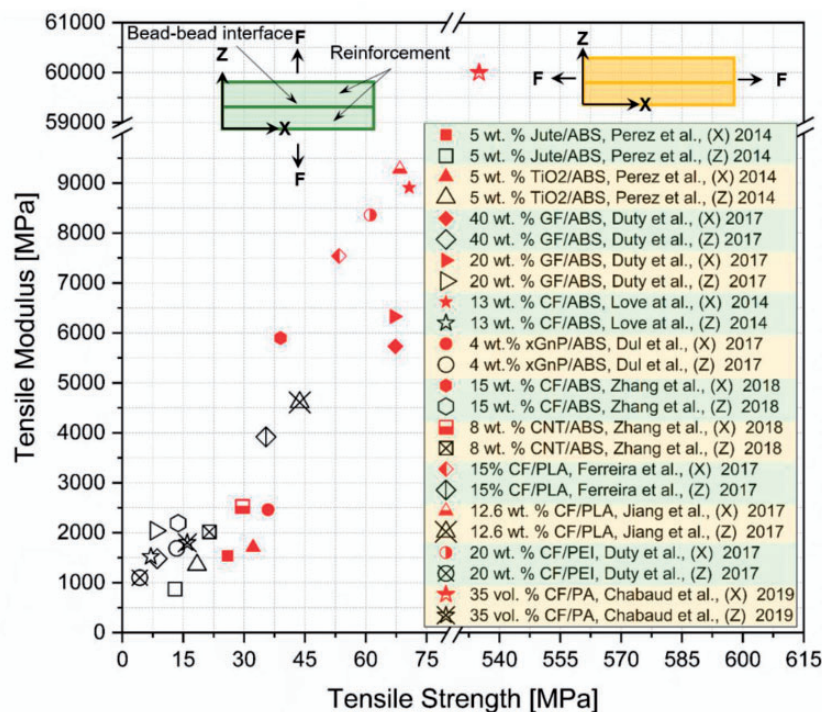


Figure 15. Comparison of x-directional and z-directional tensile properties of FFF-composites.^{61,113,127,128,131,138,158,168} The presented data covers nano, micron and continuous fiber reinforcement.

allows already cooled beads to again soften once in contact with a hot bead deposited on top of it leading to improved packing. However, at higher fiber loading, micro-voids at the fiber–matrix interface (intra-bead voids) inside single beads become more dominant. These can create fracture mechanics type stress concentrations, which cause the part to fail at lower stresses than expected. Similar stress concentration effects are also explained in terms of inter-bead voids by Tronvoll et al.¹⁶⁹

Process parameters optimization

The process parameters have a significant effect on the property of the composite parts. A good number of optimization study is found in the literature on FFF processed neat polymeric parts,^{170–176} but it is very rarely found for two-phase systems.^{177,178} In most of these studies on neat polymers, a large number of coupon testing has usually been performed by changing different FFF process parameters, and various design of experiments have been adopted such as ANOVA, Taguchi method, full factorial designs, and fuzzy logic to optimize the strength, modulus, dimensional accuracy. In all of these studies, different processing parameters like build orientation, layer height, layer thickness, processing temperature, and printing speed were usually investigated by taking 3–4 parameters at a time. A couple of studies were found from the finite element modeling (FEA) analysis, where the effect of build orientation on mechanical properties was investigated mostly by simulations.¹⁷⁹ In separate studies, few other process variables like the effect of layer orientation and part density were also investigated.^{105,180} A comprehensive literature review on the FFF process summarizes different approaches that have been adopted with different materials to optimize the structural properties and surface finish¹⁸¹ of single-phase polymers. Ning et al.⁸ conducted an experimental study with the CF/PLA composites varying the printing speed, print temperature, and layer thickness. The effects of such process parameters on tensile properties were investigated. However, the study fails to give any general guideline for the process parameters of any random two-phase system. Recently, Papon et al.¹⁸² studied the effects of process-induced variabilities on dimensional accuracy, void contents, and mechanical properties of CF/PLA composite in a multi-scale manner. The effects of dominant process parameters like solidification rate, print temperature, platform temperature, and print speed were analyzed from single bead to multi-layer end-product. The experimental observations were used to build up a physics-based surrogate model by modifying the classical lamination theory. Finally, non-intrusive polynomial chaos

(NIPC)-based stochastic uncertainty analysis was carried out on the developed model and verified with the experiment. However, the model may be good for CF/PLA system but may not be well-suited for other polymeric systems. Moreover, none of these studies looked at the bead-bead interface and fiber–matrix interface characteristics, which is significant to address the anisotropy. Thus, the need to build up a generic process model for different polymer systems and different reinforcements are yet to be fulfilled.

Fiber–matrix bonding and bead to bead bonding

It is understood by now that the two interfaces (fiber–matrix and bead-bead) have a profound impact on the properties of FFF-part. However, the interfacial properties of fiber–matrix and bead-bead have not been well investigated. The as-received reinforcements are usually inert and do not have reactive functional groups to be chemically bonded with the polymers. Hence, fiber surface modification is necessary for better wettability with the polymers. The well-established fiber-functionalization techniques¹⁸³ for traditional manufacturing processes can very well be adopted for FFF-AM. Oxidation treatment has been found to improve the interfacial strength¹²⁹ of discontinuous CF reinforced PLA composites with better stability. Similar functionalization can be done for different material systems to improve adhesion and interfacial characteristics. A preliminary study with continuous fiber reinforcement¹⁵² on the fiber surface modification of CFR-system showed improved tensile strength and flexural strength by 13.75% and 165%, respectively, with the sized fiber compared to as-received fibers. The similar approach may be adopted for the nano and micron-scaled reinforcement too. There are few works on understanding the impact strength,¹⁸⁴ inter-laminar shear strength,¹⁸⁵ inter-laminar fracture toughness.^{186,187} These studies showed that the interfacial property is very strongly dependent on the bead-bead interfacial characteristics. It is critical for the beads to maintain a temperature of above the glass transition temperature of the material to ensure good molecular diffusion at the interfaces. Different approaches may be adopted to improve the inter-bead bonding. Some of the approaches involve in-process ultrasonic vibration,¹⁸⁸ in-process laser localized pre-deposition heating,¹⁸⁹ infrared preheating of as-deposited layer,¹⁹⁰ microwave irradiation by coating the filaments with CNTs,¹⁹¹ etc. Parandoush et al.¹⁹² introduced a compaction roller like the BAAM setup of ORNL⁶¹ while laying up the beads and a laser source on top of the bead surface to keep the surface heated for better bonding with incoming beads. These studies show some enhancement in interfacial properties; however, new-sustainable methods need to be developed for

continuous improvement. The most recent advancement in FFF-printing is adopting the Z-pinning¹⁹³ technology like the traditional composite processing. The technology is developed by ORNL, and the tests showed some sparkling results by improving the z-directional strength by 3–5 times and toughness by 8 times in comparison to unpinned CF/PLA composites. However, it is still an immature technology, and the effects of bead-bead bonding, bead-pin bonding needs to be investigated for further improvement. Another exciting addition in FFF technology is the six degrees of freedom (DOF) FFF extrusion system.^{194,195} This multi-DOF extrusion system may give the flexibility to align beads with a preferred direction (x, y, and z) with the part's stress contours to arrest the inter-layer delamination like the Z-pinning. Similar technologies may be developed for woven composites too. By addressing the inherent issues and by developing new methods, FFF can very well be used as a reliable manufacturing system in the near future for industrial applications.

Artificial intelligence (AI) and integrated process-structure-property framework

The reliability of FFF composites is still questionable due to its large process variable parameters (discussed in section “Process parameters optimization”). Figure 16 shows different material and process-induced variations in the FFF-processed composites, which play the major role behind the inferior performance and lack of reliability. Thus, extensive experimental testing is required before incorporating the part into the Design Allowable Database to avoid the uncertainties in the constituent materials and manufacturing process, hence, reduce the risk of failure

in the end-use product. The knowledge of the optimal designs would allow exploring design strategies and physical insights of how to create tougher and stronger hierarchical composites.

Developing a robust AI tool can help in this respect by identifying the predictive and actionable recommendations and optimize the part quality and process design. There is still a limited scientific understanding of the FFF process (AM, in general) and structure-property relationships. In-situ process monitoring, real-time defect detection, process monitoring, validation, and certification are needed to advance the technology further, which demands advanced control and monitoring of the existing process. Advanced computational and analytical tools are needed to analyze the high dimensional and complex data sets acquired from various onboard sensors. In this regard, machine learning (ML) can offer great potential in transforming these AM data into insightful knowledge and help in decision making.¹⁹⁶ Gu et al.¹⁹⁷ proposed a convolutional neural network (CNN) based ML approach to design hierarchical materials. The AI tool was trained with hundreds of thousands of data generated from a FEA model. After training, the model predicted the mechanical properties of the hierarchical systems and generated new microstructural patterns that lead to tougher and stronger materials. The selected design was also FFF-printed and tested for characterization. The AI tool could accurately predict the tensile strength of the developed system. In a separate study, Zhang et al.¹⁹⁸ used a long short-term memory network and layer-wise relevance propagation to predict the tensile strength of the FFF printed part. The model was trained with the data generated from experimental testing of components printed with different process parameters. The developed ML algorithm was also

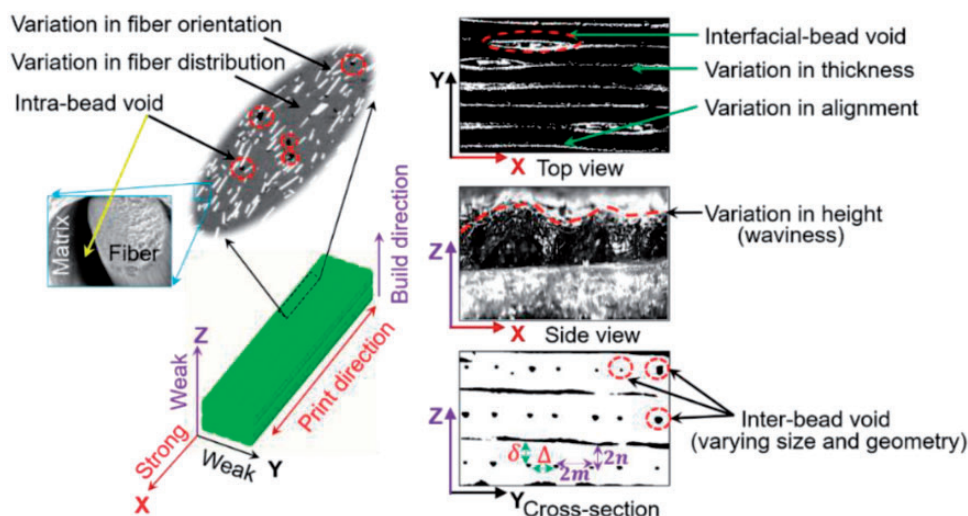


Figure 16. Material and process induced variations in FFF processed composites.¹⁸² Reproduced with permission.

compared with available support vector regression (SVR) and random forest (RF) algorithms and was found to provide a better result than SVR and RF. Rao et al.¹⁹⁹ used multiple temperature, vibration, and image sensors to study in-situ process conditions and developed a data-driven predictive model combining the nonparametric Bayesian Dirichlet process (DP) mixture model and evidence theory. Wu et al.²⁰⁰ developed another real-time process monitoring model based on the data provided by the acoustic emission sensor and used a hidden semi-Markov model to identify the process states. In a separate study, Jin et al.²⁰¹ formed another in-situ process monitoring and auto-correction model using CNN based ML technique, where the AI tool monitors the process condition and automatically tunes the process parameters if any anomaly is detected in the microstructure. All these above discussed works are very likely to be explored for fiber-reinforced composites in the near future. However, it needs a smart integration of available AM technologies and advanced analytical/computational tools. An integrated computational materials engineering (ICME) framework by combining multi-scale physics-based materials, structure, and machine-learning model is going to be one of the future thrust for the success of AM in composite industries.

4D printing in FFF and future research

In 4D printing, time is considered as the fourth dimension. Although 4D printing is mostly popular with thermoset polymers, the integration of shape-memory functionality into the FFF feedstock material can enable FFF into 4D printing capability too. The printed material can transform in a pre-programmed way in response to an external stimulus. Thermoplastic composites and complex structures with shape memory functionality are very promising for in-space applications like deployable solar panels, composite hinges, and antennas.²⁰² Shape memory polymers (SMPs) have recently been studied with FFF printers^{203–205} to understand the changes in the structure over time under the influence of external stimuli like heat. To the authors' knowledge, no such studies relating to SMPs-based composites and the status of structural performances are conducted so far. For future space explorations, in-space manufacturing is a key aspect and NASA is currently striving towards developing such in-space manufacturing lab. In such applications, FFF can be used to develop stronger, reliable, and multifunctional composites. The SMPs-based composites can add more flexibility in terms of handling and functionality in terms of performance. However, agile research efforts are needed on understanding the balance between the structural

performance and shape-memory functionality of the processed parts.

In summary, future research needs in FFF-composites are as follows:

- The through-thickness strength of the composites needs to be improved to reduce the anisotropy of parts. Since the FFF processed parts are fundamentally weak in the out-of-plane direction, this must need to be addressed through advanced process modeling, redesigning the extrusion system, and/or modification of current setup through localized heating layer by layer during printing.
- The reliability of the FFF system needs to be improved by advanced process modeling and optimization of process parameters. The FFF system must give a repeatable outcome for the reliability and commercial viability of the parts. The effects of different process variables in a multi-scale modeling paradigm need to be focused to address this issue.
- In order to achieve the greater advantage of FFF-composites, higher-length fibers (for discontinuous fiber reinforcement) and higher fiber volume fractions need to be incorporated in the FFF system. The challenges in higher-length fibers (higher than the critical fiber length) and higher volume fraction comes with the challenges in fiber dispersion, distribution, and nozzle clogging during printing.
- One of the major challenges in FFF is to improve the two distinct interfaces (interface between bead to bead and interface between the fiber and matrix). The bead to bead interface can be addressed by adopting novel techniques like localized heating, modifying the extruded bead shape, microwave heating, filament coating, etc. The fiber/matrix interfacial bonding needs to be addressed in terms of proper surface treatment of fibers, hybrid composites by growing compatible sites or CNTs on fiber surfaces, etc. before mixing with the resin material.
- In-situ process monitoring, defect detection, etc. are soon going to be interesting research focuses on FFF. The development of AI tools, the use of advanced ML techniques, integration of different sensors, and computational models with experiments to develop the ICME approach can play a vital role in the future.

Conclusion

This article summarizes the current understanding of FFF process, physical model and material development, resulting properties, knowledge gaps, and future research needs. The numerical models developed till to-date bring out some of the key findings like the physics of fiber orientation and bead spreading

architecture, solidification, deformation, and failure initiation. Despite these, there are scopes to study the bond formation mechanism to understand the bead to bead and layer-wise bonding maintaining the geometric integrity of the structure. Moreover, most of the studies on the solidification phase are conducted for single-phase polymers with the simplified fluid model. The fluid behavior may change dramatically in the case of composite materials. Thus, non-Newtonian fluid flow characteristics may need to be considered. The bead-solidification characteristics and bead-bead bonding characteristics for a two-phase material are yet to be studied. Such analysis for two-phase composite would require enormous computational power, which is still a challenge.

The current state of the art explains the material development, property enhancement, and anisotropy in the parts. The summarized tensile properties shows a lot of variabilities. Nano and short fiber reinforcement are yet to fulfill the aerospace-grade material requirement. However, the continuous fiber reinforcement shows a great promise in exceeding the expectation. Conversely, the anisotropy and weak through-thickness strength are also largely evident for the continuous fiber-reinforced system. The nano and discontinuous fiber-reinforced FFF parts have a huge potential in multifunctional applications like sensors and thermal applications. New application areas may also need to be explored apart from structural and thermal applications.

The paper reveals that some remarkable works have been done to understand the process and expand the capabilities of FFF. However, many areas are yet to be explored. A lot of experiments and numerical models are developed as preliminary works considering a simplified environment. These need to be revisited and modified based on the current fundamental understanding of the process. In conclusion, FFF of composites has already shown its potential in rapid tooling applications and is highly promising in turning to be a reliable, mainstream manufacturing method. This can only be achieved by addressing the major challenges like the formation of void contents, interfacial bonding, limitation in usable fiber length and volume fraction through an advanced process modeling, system development and ICME approach. The unique characteristic of tailorable properties cannot only contribute to the aerospace and automotive industry but also electronics, sensors, biomedical industries can be benefitted by FFF.


Declaration of conflicting interests

The author(s) declared no potential conflicts of interest with respect to the research, authorship, and/or publication of this article.

Funding

The author(s) received no financial support for the research, authorship, and/or publication of this article.

ORCID iD

Easir Arafat Papon  <https://orcid.org/0000-0001-5124-197X>

References

1. Hull CW. Apparatus for production of three-dimensional objects by stereolithography. Google Patents, 1986.
2. Sachs EM, Haggerty JS, Cima MJ, et al. Three-dimensional printing techniques. Google Patents, 1993.
3. Park J, Tari MJ and Hahn HT. Characterization of the laminated object manufacturing (LOM) process. *Rapid Prototyp J* 2000; 6: 36–50.
4. Gu D, Meiners W, Wissenbach K, et al. Laser additive manufacturing of metallic components: materials, processes and mechanisms. *Int Mater Rev* 2012; 57: 133–164.
5. Crump SS. Apparatus and method for creating three-dimensional objects. Google Patents, 1992.
6. Manapat JZ, Chen Q, Ye P, et al. 3D printing of polymer nanocomposites via stereolithography. *Macromol Mater Eng* 2017; 302: 1600553.
7. Ivanova O, Williams C and Campbell T. Additive manufacturing (AM) and nanotechnology: promises and challenges. *Rapid Prototyp J* 2013; 19: 353–364.
8. Ning F, Cong W, Qiu J, et al. Additive manufacturing of carbon fiber reinforced thermoplastic composites using fused deposition modeling. *Compos Part B Eng* 2015; 80: 369–378.
9. Wohlers Report 2018. *3D printing and additive manufacturing state of the industry: annual worldwide progress report*. USA: Wohlers Associates, 2018.
10. ASTM I. *ASTM52900-15 standard terminology for additive manufacturing—general principles—terminology*. West Conshohocken, PA: ASTM International, 2015.
11. van de Werken N, Tekinalp H, Khanbolouki P, et al. Additively manufactured carbon fiber-reinforced composites: state of the art and perspective. *Addit Manuf* 2019; 31:100962.
12. Goodridge RD, Shofner ML, Hague RJ, et al. Processing of a Polyamide-12/carbon nanofibre composite by laser sintering. *Polym Test* 2011; 30: 94–100.
13. Jansson A and Pejryd LJAM. Characterisation of carbon fibre-reinforced polyamide manufactured by selective laser sintering. *Addit Manuf* 2016; 9: 7–13.
14. Chen B, Berretta S, Evans K, et al. A primary study into graphene/polyether ether ketone (PEEK) nanocomposite for laser sintering. *Appl Surf Sci* 2018; 428: 1018–1028.
15. Yan M, Tian X, Peng G, et al. High temperature rheological behavior and sintering kinetics of CF/PEEK composites during selective laser sintering. *Compos Sci Technol* 2018; 165: 140–147.

16. Parandoush P, Zhou C and Lin D. 3D printing of ultra-high strength continuous carbon fiber composites. *Adv Eng Mater* 2019; 21: 1800622.
17. Ansys. www.ansys.com/products/structures/additive-manufacturing (accessed 1 June 2020).
18. e-Xstream engineering. www.e-xstream.com/page/additive-manufacturing (accessed 1 June 2020).
19. Simulia. www.3ds.com/products-services/simulia/trends/digital-additive-manufacturing/ (accessed 1 June 2020).
20. Love LJ. Utility of big area additive manufacturing (BAAM) for the rapid manufacture of customized electric vehicles. TN, USA: Oak Ridge, 2015.
21. DeNardo NM. *Additive manufacturing of carbon fiber-reinforced thermoplastic composites*. Theses and Dissertations, Purdue University, USA, 2016.
22. LSAM. www.thermwood.com/lam_home.htm (accessed 1 June 2020).
23. Business Journal Daily. <https://businessjournaldaily.com/strangepresse-partners-with-baylor-university/> (accessed 1 June 2020).
24. Wang X, Jiang M, Zhou Z, et al. 3D printing of polymer matrix composites: a review and prospective. *Compos Part B Eng* 2017; 110: 442–458.
25. Ngo TD, Kashani A, Imbalzano G, et al. Additive manufacturing (3D printing): a review of materials, methods, applications and challenges. *Compos Part B Eng* 2018; 143: 172–196.
26. Parandoush P and Lin D. A review on additive manufacturing of polymer-fiber composites. *Compos Struct* 2017; 182: 36–53.
27. Goh GD, Yap YL, Agarwala S, et al. Recent progress in additive manufacturing of fiber reinforced polymer composite. *Adv Mater Technol* 2019; 4: 1800271.
28. Hofstätter T, Pedersen DB, Tosello G, et al. State-of-the-art of fiber-reinforced polymers in additive manufacturing technologies. *J Reinforced Plast Compos* 2017; 36: 1061–1073.
29. Popescu D, Zapciu A, Amza C, et al. FDM process parameters influence over the mechanical properties of polymer specimens: a review. *Polym Test* 2018; 69: 157–166.
30. Mohan N, Senthil P, Vinodh S, et al. A review on composite materials and process parameters optimisation for the fused deposition modelling process. *Virtual Phys Prototyp* 2017; 12: 47–59.
31. Brenken B, Barocio E, Favaloro A, et al. Fused filament fabrication of fiber-reinforced polymers: a review. *Addit Manuf* 2018; 21: 1–16.
32. Turner BN, Strong R, Gold SA. A review of melt extrusion additive manufacturing processes: I. Process design and modeling. *Rapid Prototyp J* 2014; 20: 192–204.
33. Ramanath H, Chua C, Leong K, et al. Melt flow behaviour of poly- ϵ -caprolactone in fused deposition modelling. *J Mater Sci Mater Med* 2008; 19: 2541–2550.
34. Heller BP, Smith DE and Jack DA. Effects of extrudate swell and nozzle geometry on fiber orientation in fused filament fabrication nozzle flow. *Addit Manuf* 2016; 12: 252–264.
35. Pipes RB, Hearle J, Beaussart A, et al. A constitutive relation for the viscous flow of an oriented fiber assembly. *J Compos Mater* 1991; 25: 1204–1217.
36. Duty CE, Ajinjeru C, Kishore V, et al. *A viscoelastic model for evaluating extrusion-based print conditions*. Oak Ridge National Lab (ORNL), TN, USA: Oak Ridge, 2017.
37. Fitzharris ER, Watanabe N, Rosen DW, et al. Effects of material properties on warpage in fused deposition modeling parts. *Int J Adv Manuf Technol* 2018; 95: 2059–2070.
38. Watanabe N, Shofner M, Treat N, et al. A model for residual stress and part warpage prediction in material extrusion with application to polypropylene. In: *2016 annual international solid freeform fabrication symposium*, Austin, 2016.
39. Abbott A, Tandon G, Bradford R, et al. Process-structure-property effects on ABS bond strength in fused filament fabrication. *Addit Manuf* 2018; 19: 29–38.
40. Yunus DE, Shi W, Sohrabi S, et al. Shear induced alignment of short nanofibers in 3D printed polymer composites. *Nanotechnology* 2016; 27: 495302.
41. Yunus DE, He R, Shi W, et al. Short fiber reinforced 3d printed ceramic composite with shear induced alignment. *Ceram Int* 2017; 43: 11766–11772.
42. Yardmci A. *Process analysis and development for fused deposition*. PhD Thesis, University of Illinois at Chicago, Chicago, 1999.
43. Rodriguez MJ. *Modeling the mechanical behavior of fused deposition acrylonitrile-butadiene-styrene polymer components*. Doctoral Dissertation, University of Notre Dame, USA, 1999.
44. Bellini A. *Fused deposition of ceramics: a comprehensive experimental, analytical and computational study of material behavior, fabrication process and equipment design*. 2002.
45. Watanabe N. *Computational and experimental investigation of reinforced polymers for material extrusion additive manufacturing*. Masters Thesis, Georgia Institute of Technology, USA, 2016.
46. Mostafa N, Syed HM, Igor S, et al. A study of melt flow analysis of an ABS-Iron composite in fused deposition modelling process. *Tinshhua Sci Technol* 2009; 14: 29–37.
47. Stewart SR, Wentz JE and Allison JT. Experimental and Computational Fluid Dynamic Analysis of Melt Flow Behavior in Fused Deposition Modelling of Poly (lactic) Acid. In: *ASME 2015 International Mechanical Engineering Congress and Exposition*. American Society of Mechanical Engineers, 2015.
48. Papon EA, Haque A and Sharif MAR. *Effect of nozzle geometry on melt flow simulation and structural property of thermoplastic nanocomposites in fused deposition modeling*. In: *Proceeding of the American society for composites, Thirty-second technical conference*, 2017.
49. Kim T, Trangkanukulkij R and Kim WS. Nozzle shape guided filler orientation in 3D printed photo-curable nanocomposites. *Sci Rep* 2018; 8: 3805.

50. Osswald TA, Puentes J and Kattinger J. Fused filament fabrication melting model. *Addit Manuf* 2018; 22: 51–59.
51. Nixon J, Dryer B, Lempert I, et al. Three parameter analysis of fiber orientation in fused deposition modeling geometries. In: *Proceedings of PPS conference*, Las Vegas, Nevada, USA, 28–30 April 2014.
52. Garcia A. *Nozzle geometry effects on exit orientation of short fiber composites*. Kansas: Wichita State University, 2017.
53. Folgar F and Tucker CL III. Orientation behavior of fibers in concentrated suspensions. *J Reinforced Plast Compos* 1984; 3: 98–119.
54. Advani SG and Tucker CL III. The use of tensors to describe and predict fiber orientation in short fiber composites. *J Rheol* 1987; 31: 751–784.
55. Wang Z and Smith D. Rheology effects on predicted fiber orientation and elastic properties in large scale polymer composite additive manufacturing. *J Compos Sci* 2018; 2: 10.
56. Wang Z and Smith DE. Numerical analysis of screw swirling effects on fiber orientation in large area additive manufacturing polymer composite deposition. *Compos Part B Eng* 2019; 177: 107284.
57. Lewicki JP, Rodriguez JN, Zhu C, et al. 3D-printing of meso-structurally ordered carbon fiber/polymer composites with unprecedented orthotropic physical properties. *Sci Rep* 2017; 7: 43401.
58. Bertevas E, Férec J, Khoo BC, et al. Smoothed particle hydrodynamics (SPH) modeling of fiber orientation in a 3D printing process. *Phys Fluids* 2018; 30: 103103.
59. Yang D, Wu K, Wan L, et al. A particle element approach for modelling the 3D printing process of fibre reinforced polymer composites. *J Manuf Mater Process* 2017; 1: 10.
60. Heller BP, Smith DE and Jack DA. Planar deposition flow modeling of fiber filled composites in large area. *Addit Manuf* 2019; 25: 227–238.
61. Duty CE, Kunc V, Compton B, et al. Structure and mechanical behavior of big area additive manufacturing (BAAM) materials. *Rapid Prototyp J* 2017; 23: 181–189.
62. Tekinalp HL, Kunc V, Velez-Garcia GM, et al. Highly oriented carbon fiber–polymer composites via additive manufacturing. *Compos Sci Technol* 2014; 105: 144–150.
63. Mulholland T, Goris S, Boxleitner J, et al. Process-induced fiber orientation in fused filament fabrication. *J Compos Sci* 2018; 2: 45.
64. Russell T, Heller B, Jack DA, et al. Prediction of the fiber orientation state and the resulting structural and thermal properties of fiber reinforced additive manufactured composites fabricated using the big area additive manufacturing process. *J Compos Sci* 2018; 2: 26.
65. Furlani EP, Sukhotskiy V, Verma A, et al. Numerical simulation of extrusion additive manufacturing: fused deposition modeling. *Inf Electron Microsyst TechConnect Brief* 2018; 118–121.
66. Ravoori D, Lowery C, Prajapati H, et al. Experimental and theoretical investigation of heat transfer in platform bed during polymer extrusion based additive manufacturing. *Polym Test* 2019; 73: 439–446.
67. Xia H, Lu J, Dabiri S, et al. Fully resolved numerical simulations of fused deposition modeling. Part I: fluid flow. *Rapid Prototyp J* 2018; 24: 463–476.
68. Comminal R, Serdeczny MP, Pedersen DB, et al. Numerical modeling of the strand deposition flow in extrusion-based additive manufacturing. *Addit Manuf* 2018; 20: 68–76.
69. Serdeczny MP, Comminal R, Pedersen DB, et al. Experimental validation of a numerical model for the strand shape in material extrusion additive manufacturing. *Addit Manuf* 2018; 24: 145–153.
70. Serdeczny MP, Comminal R, Pedersen DB, et al. Numerical prediction of the porosity of parts fabricated with fused deposition modeling. In: *29th annual international solid freeform fabrication symposium (SFF Symp 2018)*, Austin, United States, 2018.
71. Comminal R, Serdeczny M, Pedersen D, et al. Laboratory for freeform fabrication. In: *29th Annual international solid freeform fabrication symposium (SFF Symp 2018)*, Austin, Texas, USA, 13–15 August 2018.
72. Balani SB, Chabert F, Nassiet V, et al. Influence of printing parameters on the stability of deposited beads in fused filament fabrication of poly (lactic) acid. *Addit Manuf* 2019; 25: 112–121.
73. Balani SB, Arthur C, France C, et al. Influence of parameters controlling the extrusion step in fused filament fabrication (FFF) process applied to polymers using numerical simulation. *AIP Conf Proc* 2018; 1960: 140003.
74. Liu J, Anderson KL and Sridhar N. Direct simulation of polymer fused deposition modeling (FDM)—an implementation of the multi-phase viscoelastic solver in OpenFOAM. *Int J Comput Methods* 2018; 17: 1844002.
75. Atif Yardimci M, Hattori T, Guceri SI, et al. Thermal analysis of fused deposition. *Int Solid Freeform Fabrication Symposium*. 1997.
76. Brenken B, Favaloro A, Barocio E, et al. Development of a model to predict temperature history and crystallization behavior of 3D printed parts made from fiber-reinforced thermoplastic polymers. In: *SAMPE conference, Long Beach, CA*, 2016.
77. Zhou Y, Nyberg T, Xiong G, et al. Temperature analysis in the fused deposition modeling process. In: *2016 3rd international conference on information science and control engineering (ICISCE)*, IEEE, 2016.
78. Pooladvand K and Furlong C. Thermo-mechanical investigation of fused deposition modeling by computational and experimental methods. *Mech Compos Multifunct Mater* 2017; 7: 45–54.
79. Xia H, Lu J and Tryggvason G. A numerical study of the effect of viscoelastic stresses in fused filament fabrication. *Comput Methods Appl Mech Eng* 2019; 346: 242–259.
80. Likhtman AE and Graham RS. Simple constitutive equation for linear polymer melts derived from molecular theory: Rolie–Poly equation. *J Non-Newton Fluid Mech* 2003; 114: 1–12.
81. Compton BG, Post BK, Duty CE, et al. Thermal analysis of additive manufacturing of large-scale

- thermoplastic polymer composites. *Addit Manuf* 2017; 17: 77–86.
82. Talagani M, DorMohammadi S, Dutton R, et al. Numerical simulation of big area additive manufacturing (3D printing) of a full size car. *SAMPE J* 2015; 27: 36.
 83. Favaloro AJ, Brenken B, Barocio E, et al. Simulation of polymeric composites additive manufacturing using Abaqus. In: *Proceedings of the Dassault Systemes' Science in the Age of Experience*, Chicago, IL, 15–18 May 2017.
 84. Spinnie NK. *Large scale fused deposition modeling: the effect of process parameters on bead geometry*. PhD Thesis, Virginia Tech, 2016.
 85. Bellehumeur C, Li L, Sun Q, et al. Modeling of bond formation between polymer filaments in the fused deposition modeling process. *J Manuf Process* 2004; 6: 170–178.
 86. Sun Q. *Bond formation between polymer filaments in fused deposition modeling process*. Calgary: University of Calgary, 2005.
 87. Shahriar BB, France C, Valerie N, et al. Toward improvement of the properties of parts manufactured by FFF (fused filament fabrication) through understanding the influence of temperature and rheological behaviour on the coalescence phenomenon. *AIP Conf Proc* 2017; 1896: 040008.
 88. Sun Q, Rizvi G, Bellehumeur C, et al. Effect of processing conditions on the bonding quality of FDM polymer filaments. *Rapid Prototyp J* 2008; 14: 72–80.
 89. Gurralla PK and Regalla SP. *Part strength evolution with bonding between filaments in fused deposition modeling. This paper studies how coalescence of filaments contributes to the strength of final FDM part*. *Virtual Phys Prototyp* 2014; 9: 141–149.
 90. Costa S, Duarte F and Covas J. Towards modelling of free form extrusion: analytical solution of transient heat transfer. *Int J Mater Form* 2008; 1: 703–706.
 91. Costa S, Duarte F and Covas J. Estimation of filament temperature and adhesion development in fused deposition techniques. *J Mater Process Technol* 2017; 245: 167–179.
 92. McIlroy C and Graham R. Modelling flow-enhanced crystallisation during fused filament fabrication of semi-crystalline polymer melts. *Addit Manuf* 2018; 24: 323–340.
 93. McIlroy C and Olmsted P. Disentanglement effects on welding behaviour of polymer melts during the fused-filament-fabrication method for additive manufacturing. *Polymer* 2017; 123: 376–391.
 94. McIlroy C and Olmsted PD. Deformation of an amorphous polymer during the fused-filament-fabrication method for additive manufacturing. *J Rheol* 2017; 61: 379–397.
 95. Barocio E, Brenken B, Favaloro A, et al. Fusion bonding simulations of semi-crystalline polymer composites in the extrusion deposition additive manufacturing process. In: *Proceedings of the American Society for Composites—Thirty-second Technical Conference*, West Lafayette, IN, USA, 23–25 October 2017.
 96. Drummer D, Cifuentes-Cuellar S and Rietzel D. Suitability of PLA/TCP for fused deposition modeling. *Rapid Prototyp J* 2012; 18: 500–507.
 97. Gnanasekaran K, Heijmans T, Van Bennekom S, et al. 3D printing of CNT-and graphene-based conductive polymer nanocomposites by fused deposition modeling. *Appl Mater Today* 2017; 9: 21–28.
 98. Li H, Zhang S, Yi Z, et al. Bonding quality and fracture analysis of polyamide 12 parts fabricated by fused deposition modeling. *Rapid Prototyp J* 2017; 23: 973–982.
 99. Wu W, Geng P, Li G, et al. Influence of layer thickness and raster angle on the mechanical properties of 3D-printed PEEK and a comparative mechanical study between PEEK and ABS. *Materials (Basel)* 2015; 8: 5834–5846.
 100. Wang T-M, Xi J-T and Jin Y. A model research for prototype warp deformation in the FDM process. *Int J Adv Manuf Technol* 2007; 33: 1087–1096.
 101. Xinhua L, Shengpeng L, Zhou L, et al. An investigation on distortion of PLA thin-plate part in the FDM process. *Int J Adv Manuf Technol* 2015; 79: 1117–1126.
 102. Wijnen B, Sanders P and Pearce JM. Improved model and experimental validation of deformation in fused filament fabrication of polylactic acid. *Prog Addit Manuf* 2018; 3: 193–203.
 103. Armillotta A, Bellotti M and Cavallaro M. Warpage of FDM parts: Experimental tests and analytic model. *Robot Comput Int Manuf* 2018; 50: 140–152.
 104. Zhang Y and Chou K. A parametric study of part distortions in fused deposition modelling using three-dimensional finite element analysis. *Proc Inst Mech Eng Part B J Eng Manuf* 2008; 222: 959–968.
 105. Zhang Y and Chou Y. Three-dimensional finite element analysis simulations of the fused deposition modelling process. *Proc Inst Mech Eng Part B J Eng Manuf* 2006; 220: 1663–1671.
 106. Xia H, Lu J and Tryggvason G. Fully resolved numerical simulations of fused deposition modeling. Part II—solidification, residual stresses and modeling of the nozzle. *Rapid Prototyp J* 2018; 24: 973–987.
 107. Xia H, Lu J and Tryggvason G. Simulations of fused filament fabrication using a front tracking method. *Int J Heat Mass Transf* 2019; 138: 1310–1319.
 108. Du J, Wei Z, Wang X, et al. An improved fused deposition modeling process for forming large-size thin-walled parts. *J Mater Process Technol* 2016; 234: 332–341.
 109. Cattenone A, Morganti S, Alaimo G, et al. Finite element analysis of additive manufacturing based on fused deposition modeling: distortions prediction and comparison with experimental data. *J Manuf Sci Eng* 2019; 141: 011010.
 110. Shofner M, Rodríguez-Maciás F, Vaidyanathan R, et al. Single wall nanotube and vapor grown carbon fiber reinforced polymers processed by extrusion free-form fabrication. *Compos Part A Appl Sci Manuf* 2003; 34: 1207–1217.
 111. Dorigato A, Moretti V, Dul S, et al. Electrically conductive nanocomposites for fused deposition modelling. *Synth Met* 2017; 226: 7–14.

112. Dul S, Fambri L and Pegoretti A. Filaments production and fused deposition modelling of ABS/carbon nanotubes composites. *Nanomaterials* 2018; 8: 49.
113. Zhang W, Cotton C, Sun J, et al. Interfacial bonding strength of short carbon fiber/acrylonitrile-butadiene-styrene composites fabricated by fused deposition modeling. *Compos Part B Eng* 2018; 137: 51–59.
114. Patanwala HS, Hong D, Vora SR, et al. The microstructure and mechanical properties of 3D printed carbon nanotube-poly(lactic acid) composites. *Polym Compos* 2018; 39: E1060–E1071.
115. Lebedev S, Gefle O, Amitov E, et al. Mechanical properties of PLA-based composites for fused deposition modeling technology. *Int J Adv Manuf Technol* 2018; 97: 511–518.
116. Nadernezhad A, Unal S, Khani N, et al. Material extrusion-based additive manufacturing of structurally controlled poly (lactic acid)/carbon nanotube nanocomposites. *Int J Adv Manuf Technol* 2019; 102: 1–14.
117. Gonçalves J, Lima P, Krause B, et al. Electrically conductive polyetheretherketone nanocomposite filaments: from production to fused deposition modeling. *Polymers* 2018; 10: 925.
118. Kalia K and Ameli A. Tensile Properties of 3D-Printed Polycarbonate/Carbon Nanotube Nanocomposites. In: *ASME 2018 conference on smart materials, adaptive structures and intelligent systems*, San Antonio, Texas, USA, 10–12 September 2018. American Society of Mechanical Engineers.
119. Papon EA and Haque A. Tensile properties, void contents, dispersion and fracture behaviour of 3D printed carbon nanofiber reinforced composites. *J Reinforced Plast Compos* 2018; 37: 381–395.
120. Aumnate C, Pongwisuthiruchte A, Pattananuwat P, et al. Fabrication of ABS/graphene oxide composite filament for fused filament fabrication (FFF) 3D printing. *Adv Mater Sci Eng* 2018; 2018:9.
121. Dul S, Fambri L, Merlini C, et al. Effect of graphene nanoplatelets structure on the properties of acrylonitrile-butadiene-styrene composites. *Polym Compos* 2017; 40: E285–E300.
122. Zhu D, Ren Y, Liao G, et al. Thermal and mechanical properties of polyamide 12/graphene nanoplatelets nanocomposites and parts fabricated by fused deposition modeling. *J Appl Polym Sci* 2017; 134: 45332.
123. Coppola B, Cappetti N, Maio LD, et al. 3D printing of PLA/clay nanocomposites: influence of printing temperature on printed samples properties. *Materials* 2018; 11: 1947.
124. Es-Said O, Foyos J, Noorani R, et al. Effect of layer orientation on mechanical properties of rapid prototyped samples. *Mater Manuf Process* 2000; 15: 107–122.
125. Berretta S, Davies R, Shyng Y, et al. Fused deposition modelling of high temperature polymers: exploring CNT PEEK composites. *Polym Test* 2017; 63: 251–262.
126. Xu Y, Wu X, Guo X, et al. The boom in 3D-printed sensor technology. *Sensors* 2017; 17: 1166.
127. Love LJ, Kunc V, Rios O, et al. The importance of carbon fiber to polymer additive manufacturing. *J Mater Res* 2014; 29: 1893–1898.
128. Jiang D and Smith DE. Anisotropic mechanical properties of oriented carbon fiber filled polymer composites produced with fused filament fabrication. *Addit Manuf* 2017; 18: 84–94.
129. Papon EA, Haque A and Spear SK. Effects of fiber surface treatment and nozzle geometry in structural properties of additively manufactured two-phase composites. In: *AIAA Scitech 2019 Forum*, San Diego, California, 7–11 January 2019.
130. Sang L, Han S, Li Z, et al. Development of short basalt fiber reinforced polylactide composites and their feasible evaluation for 3D printing applications. *Compos Part B Eng* 2019; 164: 629–639.
131. Ferreira RTL, Amatte IC, Dutra TA, et al. Experimental characterization and micrography of 3D printed PLA and PLA reinforced with short carbon fibers. *Compos Part B Eng* 2017; 124: 88–100.
132. Ivey M, Melenka GW, Carey JP, et al. Characterizing short-fiber-reinforced composites produced using additive manufacturing. *Adv Manuf Polym Compos Sci* 2017; 3: 81–91.
133. Li Y, Gao S, Dong R, et al. Additive Manufacturing of PLA and CF/PLA Binding Layer Specimens via Fused Deposition Modeling. *J Mater Eng Perform* 2018; 27: 492–500.
134. Liao G, Li Z, Cheng Y, et al. Properties of oriented carbon fiber/polyamide 12 composite parts fabricated by fused deposition modeling. *Mater Des* 2018; 139: 283–292.
135. Yu Z, Bai Y, Li Y, et al. Fiber length distribution and thermal, mechanical and morphological properties of thermally conductive polycarbonate/chopped carbon fiber composites. *Polym Int* 2018; 67: 1137–1144.
136. Chuang KC, Grady JE, Draper RD, et al. Additive manufacturing and characterization of Ultem polymers and composites. In: *CAMX conference proceedings*, Dallas, TX, 26–29 October 2015.
137. Shofner M, Lozano K, Rodríguez F, et al. Nanofiber reinforced polymers prepared by fused deposition modeling. *J Appl Polym Sci* 2003; 89: 3081–3090.
138. Perez ART, Roberson DA and Wicker RB. Fracture surface analysis of 3D-printed tensile specimens of novel ABS-based materials. *J Fail Anal Preven* 2014; 14: 343–353.
139. Li X, Ni Z, Bai S, et al. Preparation and mechanical properties of fiber reinforced PLA for 3D printing materials. *IOP Conf Ser Mater Sci Eng* 2018; 322.
140. Milosevic M, Stoof D and Pickering K. Characterizing the mechanical properties of fused deposition modelling natural fiber recycled polypropylene composites. *J Compos Sci* 2017; 1: 7.
141. Papon EA and Haque A. Fracture toughness of additively manufactured carbon fiber reinforced composites. *Addit Manuf* 2019; 26: 41–52.
142. Markforged. <https://markforged.com/materials/carbon-fiber/> (accessed 1 June 2020).
143. Van Der Klift F, Koga Y, Todoroki A, et al. 3D printing of continuous carbon fibre reinforced thermo-plastic (CFRTP) tensile test specimens. *Open J Compos Mater* 2016; 6: 18–27.

144. Melenka GW, Cheung BK, Schofield JS, et al. Evaluation and prediction of the tensile properties of continuous fiber-reinforced 3D printed structures. *Compos Struct* 2016; 153: 866–875.
145. Dickson AN, Barry JN, McDonnell KA, et al. Fabrication of continuous carbon, glass and Kevlar fibre reinforced polymer composites using additive manufacturing. *Addit Manuf* 2017; 16: 146–152.
146. Goh G, Dikshit V, Nagalingam A, et al. Characterization of mechanical properties and fracture mode of additively manufactured carbon fiber and glass fiber reinforced thermoplastics. *Mater Des* 2018; 137: 79–89.
147. Lozada JN, Ahuett-Garza H, Castañón PO, et al. Tensile properties and failure behavior of chopped and continuous carbon fiber composites produced by additive manufacturing. *Addit Manuf* 2019; 26: 227–241.
148. Oztan C, Karkkainen R, Fittipaldi M, et al. Microstructure and mechanical properties of three dimensional-printed continuous fiber composites. *J Compos Mater* 2019; 53: 271–280.
149. Dong G, Tang Y, Li D, et al. Mechanical properties of continuous Kevlar fiber reinforced composites fabricated by fused deposition modeling process. *Proc Manuf* 2018; 26: 774–781.
150. Justo J, Távara L, García-Guzmán L, et al. Characterization of 3D printed long fibre reinforced composites. *Compos Struct* 2018; 185: 537–548.
151. Matsuzaki R, Ueda M, Namiki M, et al. Three-dimensional printing of continuous-fiber composites by in-nozzle impregnation. *Sci Rep* 2016; 6: 23058.
152. Li N, Li Y and Liu S. Rapid prototyping of continuous carbon fiber reinforced polylactic acid composites by 3D printing. *J Mater Process Technol* 2016; 238: 218–225.
153. Tian X, Liu T, Wang Q, et al. Recycling and remanufacturing of 3D printed continuous carbon fiber reinforced PLA composites. *J Clean Prod* 2017; 142: 1609–1618.
154. Akhoundi B, Behraves AH and Bagheri Saed A. Improving mechanical properties of continuous fiber-reinforced thermoplastic composites produced by FDM 3D printer. *J Reinforced Plast Compos* 2019; 38: 99–116.
155. Bettini P, Alitta G, Sala G, et al. Fused deposition technique for continuous fiber reinforced thermoplastic. *J Mater Eng Perform* 2017; 26: 843–848.
156. Baumann F, Scholz J and Fleischer J. Investigation of a new approach for additively manufactured continuous fiber-reinforced polymers. *Proc CIRP* 2017; 66: 323–328.
157. Yang C, Tian X, Liu T, et al. 3D printing for continuous fiber reinforced thermoplastic composites: mechanism and performance. *Rapid Prototyp J* 2017; 23: 209–215.
158. Chabaud G, Castro M, Denoual C, et al. Hygromechanical properties of 3D printed continuous carbon and glass fibre reinforced polyamide composite for outdoor structural applications. *Addit Manuf* 2019; 26: 94–105.
159. Arevo. <https://arevo.com/2018/11/12/composite-3d-printing-debugged/> (accessed on 1 June, 2020)
160. Starke EA Jr and Staley JT. Application of modern aluminum alloys to aircraft. *Prog Aerospace Sci* 1996; 32: 131–172.
161. Nawafleh N and Celik E. Additive manufacturing of short fiber reinforced thermoset composites with unprecedented mechanical performance. *Mismatch J. Addit Manuf* 2020; 33: 101109.
162. Nusser K, Schneider GJ, Pyckhout-Hintzen W, et al. Viscosity decrease and reinforcement in polymer–silsesquioxane composites. *Macromolecules* 2011; 44: 7820–7830.
163. Chatterjee S, Nafezarefi F, Tai N, et al. Size and synergy effects of nanofiller hybrids including graphene nanoplatelets and carbon nanotubes in mechanical properties of epoxy composites. *Carbon* 2012; 50: 5380–5386.
164. Uddin MF and Sun C-T. *Major accomplishments in composite materials and sandwich structures*. Berlin, Germany: Springer, 2009, p.693–715.
165. Ma X, Zare Y and Rhee KY. A two-step methodology to study the influence of aggregation/agglomeration of nanoparticles on Young's modulus of polymer nanocomposites. *Nanoscale Res Lett* 2017; 12: 621.
166. Ashraf MA, Peng W, Zare Y, et al. Effects of size and aggregation/agglomeration of nanoparticles on the interfacial/interphase properties and tensile strength of polymer nanocomposites. *Nanoscale Res Lett* 2018; 13: 214.
167. Ferdous SF, Sarker MF and Adnan AJP. Role of nanoparticle dispersion and filler-matrix interface on the matrix dominated failure of rigid C60-PE nanocomposites: a molecular dynamics simulation study. *Polymer* 2013; 54: 2565–2576.
168. Dul S, Fambri L and Pegoretti A. Fused deposition modelling with ABS–graphene nanocomposites. *Compos Part A Appl Sci Manuf* 2016; 85: 181–191.
169. Tronvoll SA, Welo T and Elverum CW. The effects of voids on structural properties of fused deposition modelled parts: a probabilistic approach. *Int J Adv Manuf Technol* 2018; 97: 3607–3618.
170. Tandon G, Whitney T, Gerzeski R, et al. Process parameter effects on interlaminar fracture toughness of FDM printed coupons. *Mech Compos Multifunctional Mater* 2017; 7: 63–71.
171. Li H, Wang T, Sun J, et al. The effect of process parameters in fused deposition modelling on bonding degree and mechanical properties. *Rapid Prototyp J* 2018; 24: 80–92.
172. Gebisa AW and Lemu HG. Investigating effects of fused-deposition modeling (FDM) processing parameters on flexural properties of ULTEM 9085 using designed experiment. *Materials* 2018; 11: 500.
173. Mohamed OA, Masood SH and Bhowmik JL. Mathematical modeling and FDM process parameters optimization using response surface methodology based on Q-optimal design. *Appl Math Model* 2016; 40: 10052–10073.
174. Torres J, Cole M, Owji A, et al. An approach for mechanical property optimization of fused deposition modeling with polylactic acid via design of experiments. *Rapid Prototyp J* 2016; 22: 387–404.

175. Padhi SK, Sahu RK, Mahapatra S, et al. Optimization of fused deposition modeling process parameters using a fuzzy inference system coupled with Taguchi philosophy. *Adv Manuf* 2017; 5: 231–242.
176. Dong G, Wijaya G, Tang Y, et al. Optimizing process parameters of fused deposition modeling by Taguchi method for the fabrication of lattice structures. *Addit Manuf* 2018; 19: 62–72.
177. Ning F, Cong W, Hu Y, et al. Additive manufacturing of carbon fiber-reinforced plastic composites using fused deposition modeling: effects of process parameters on tensile properties. *J Compos Mater* 2017; 51: 451–462.
178. Papon EA, Mulani SB and Haque A. Optimization and polynomial chaos-based uncertainty analysis of additively manufactured polymer composites. In: *Proceedings of the American society for composites—thirty-third technical conference*. Seattle, WA, USA, 2018.
179. Domingo-Espin M, Puigoriol-Forcada JM, Garcia-Granada A-A, et al. Mechanical property characterization and simulation of fused deposition modeling polycarbonate parts. *Mater Des* 2015; 83: 670–677.
180. Farbman D and McCoy C. Materials testing of 3D printed ABS and PLA samples to guide mechanical design. In: *ASME 2016 11th International Manufacturing Science and Engineering Conference*. American Society of Mechanical Engineers, 2016.
181. Mohamed OA, Masood SH and Bhowmik JL. Optimization of fused deposition modeling process parameters: a review of current research and future prospects. *Adv Manuf* 2015; 3: 42–53.
182. Papon EA, Haque A and Mulani SB. Process optimization and stochastic modeling of void contents and mechanical properties in additively manufactured composites. *Compos Part B Eng* 2019; 177: 107325.
183. Tang LG and Kardos JL. A review of methods for improving the interfacial adhesion between carbon fiber and polymer matrix. *Polym Compos* 1997; 18: 100–113.
184. Caminero M, Chacón J, García-Moreno I, et al. Impact damage resistance of 3D printed continuous fibre reinforced thermoplastic composites using fused deposition modelling. *Compos Part B Eng* 2018; 148: 93–103.
185. Caminero M, Chacón J, García-Moreno I, et al. Interlaminar bonding performance of 3D printed continuous fibre reinforced thermoplastic composites using fused deposition modelling. *Polym Test* 2018; 68: 415–423.
186. Young D, Wetmore N and Czabaj M. Interlayer fracture toughness of additively manufactured unreinforced and carbon-fiber-reinforced acrylonitrile butadiene styrene. *Addit Manuf* 2018; 22: 508–515.
187. Ferrell WH and TerMaath SC. *Print parameter effects on the fracture properties of fiber reinforced ABS composites fabricated through fused deposition modeling*. San Diego, California: AIAA Scitech, 2019.
188. Tofangchi A, Han P, Izquierdo J, et al. Effect of ultrasonic vibration on interlayer adhesion in fused filament fabrication 3D printed ABS. *Polymers* 2019; 11: 315.
189. Ravi AK, Deshpande A and Hsu KH. An in-process laser localized pre-deposition heating approach to inter-layer bond strengthening in extrusion based polymer additive manufacturing. *J Manuf Process* 2016; 24: 179–185.
190. Kishore V, Ajinjeru C, Nycz A, et al. Infrared preheating to improve interlayer strength of big area additive manufacturing (BAAM) components. *Addit Manuf* 2017; 14: 7–12.
191. Sweeney CB, Lackey BA, Pospisil MJ, et al. Welding of 3D-printed carbon nanotube–polymer composites by locally induced microwave heating. *Sci Adv* 2017; 3: e1700262.
192. Parandoush P, Tucker L, Zhou C, et al. Laser assisted additive manufacturing of continuous fiber reinforced thermoplastic composites. *Mater Des* 2017; 131: 186–195.
193. Duty C, Failla J, Kim S, et al. Z-pinning approach for 3D printing mechanically isotropic materials. *Addit Manuf* 2019; 27: 175–184.
194. Kubalak JR, Mansfield CD, Pesek TH, et al. Design and realization of a 6 degree of freedom robotic extrusion platform. In: *Solid freeform fabrication symposium*, Austin, Texas, USA, 2016.
195. Kubalak JR, Wicks AL and Williams CB. Using multi-axis material extrusion to improve mechanical properties through surface reinforcement. *Virtual Phys Prototyp* 2018; 13: 32–38.
196. Razvi SS, Feng S, Narayanan A, et al. *A Review of Machine Learning Applications in Additive Manufacturing*. In: *ASME 2019 international design engineering technical conferences and computers and information in engineering conference*. American Society of Mechanical Engineers Digital Collection, 2019.
197. Gu GX, Chen C-T, Richmond DJ, et al. Bioinspired hierarchical composite design using machine learning: simulation, additive manufacturing, and experiment. *Mater Horizons* 2018; 5: 939–945.
198. Zhang J, Wang P and Gao RX. Deep learning-based tensile strength prediction in fused deposition modeling. *Comput Ind* 2019; 107: 11–21.
199. Rao PK, Liu JP, Roberson D, et al. Online real-time quality monitoring in additive manufacturing processes using heterogeneous sensors. *J Manuf Sci Eng* 2015; 137: 061007.
200. Wu H, Yu Z and Wang Y. Real-time FDM machine condition monitoring and diagnosis based on acoustic emission and hidden semi-Markov model. *Int J Adv Manuf Technol* 2017; 90: 2027–2036.
201. Jin Z, Zhang Z and Gu GX. Autonomous in-situ correction of fused deposition modeling printers using computer vision and deep learning. *Manuf Lett* 2019; 22: 11–15.

202. Mitchell A, Lafont U, Hołyńska M, et al. Additive manufacturing—A review of 4D printing and future applications. *Addit Manuf* 2018; 24: 606–626.
203. Yang Y, Chen Y, Wei Y, et al. 3D printing of shape memory polymer for functional part fabrication. 2016; 84: 2079–2095.
204. Hu G, Damanpack A, Bodaghi M, et al. Structures, Increasing dimension of structures by 4D printing shape memory polymers via fused deposition modeling. *Int J Adv Manuf Technol* 2017; 26: 125023.
205. Ly ST and Kim M-G. Technology, 4D printing—fused deposition modeling printing with thermal-responsive shape memory polymers. *International Journal of Precision Engineering and Manufacturing-Green Technology* 2017; 4: 267–272.